Recent Intensified Influence of the Winter North Pacific Sea Surface Temperature on the Mei-Yu Withdrawal Date

HUA LI,[a,b,c] SHENGPING HE,[d,a] KE FAN,[b,e,f] YONG LIU,[b] AND XING YUAN[c]

[a] *Collaborative Innovation Center on Forecast and Evaluation of Meteorological Disasters/Key Laboratory of Meteorological Disaster, Ministry of Education/Joint International Research Laboratory of Climate and Environment Change, Nanjing University of Information Science and Technology, Nanjing, China*
[b] *Nansen-Zhu International Research Centre, Institute of Atmospheric Physics, Chinese Academy of Sciences, Beijing, China*
[c] *School of Hydrology and Water Resources, Nanjing University of Information Science and Technology, Nanjing, China*
[d] *Geophysical Institute, University of Bergen and Bjerknes Centre for Climate Research, Bergen, Norway*
[e] *School of Atmospheric Sciences and Guangdong Province Key Laboratory for Climate Change and Natural Disasters Studies, Sun Yat-sen University, Guangzhou, China*
[f] *Southern Laboratory of Ocean Science and Engineering (Zhuhai), Zhuhai, China*

(Manuscript received 13 October 2019, in final form 23 January 2021)

ABSTRACT: The mei-yu withdrawal date (MWD) is a crucial indicator of flood/drought conditions over East Asia. It is characterized by a strong interannual variability, but its underlying mechanism remains unknown. We investigated the possible effects of the winter sea surface temperature (SST) in the North Pacific Ocean on the MWD on interannual to interdecadal time scales. Both our observations and model results suggest that the winter SST anomalies associated with the MWD are mainly contributed to by a combination of the first two leading modes of the winter SST in the North Pacific, which have a horseshoe shape (the NPSST). The statistical results indicate that the intimate linkage between the NPSST and the MWD has intensified since the early 1990s. During the time period 1990–2016, the NPSST-related SST anomalies persisted from winter to the following seasons and affected the SST over the tropical Pacific in July. Subsequently, the SST anomalies throughout the North Pacific strengthened the southward migration of the East Asian jet stream (EAJS) and the southward and westward displacement of the western North Pacific subtropical high (WPSH), leading to an increase in mei-yu rainfall from 1 to 20 July. More convincingly, the anomalous EAJS and WPSH induced by the SST anomalies can be reproduced well by numerical simulations. By contrast, the influence of the NPSST on the EASJ and WPSH were not clear between 1961 and 1985. This study further illustrates that the enhanced interannual variability of the NPSST may be attributed to the more persistent SST anomalies during the time period 1990–2016.

KEYWORDS: Mei-yu fronts; Monsoons; Precipitation; Air-sea interaction; Climate variability; Climate models

1. Introduction

In addition to the northward advance of the East Asian summer monsoon (EASM) after its onset in May, the rainy season over eastern China experiences two abrupt northward-jump periods and three stagnation periods (Tao and Chen 1987; Wang and LinHo 2002). The three latter periods consist of the first rainy period over south China, the mei-yu over the Yangtze–Huaihe River basin (YHRB; shown in Fig. 1), and the rainy period over North and Northeast China (Gu et al. 2018; Guo and Wang 1981), which correspond to three stages during the northward shift of the EASM (Ding 1992; Ding and Chan 2005). The mei-yu denotes the monsoon rainy season that occurs from mid-June to early July over the YHRB, Japan, and the southern Korean Peninsula (Ding et al. 2007; Li et al. 2019; Tanaka 1992). The mei-yu season is dominated by persistent rainy events and is characterized by a short period with heavy rainfall (Ding et al. 2007; Li and Zhang 2014; Wang et al. 2005). The mei-yu rainfall has a strong interannual variability that is closely related to flood and drought disasters in these regions (Liu et al. 2013; Qian et al. 2008).

Numerous studies have explored the impact of large-scale atmospheric circulations, the sea surface temperature (SST), and atmospheric teleconnections on mei-yu rainfall (Choi et al. 2019; Du et al. 2017; Enomoto et al. 2003; Gu et al. 2009; Huang 1992; Li et al. 2019; Wang and Wang 2018; Xie et al. 2009; Ye and Chen 2019), but there has been limited research on the mei-yu withdrawal date (MWD). The MWD has strong interannual variability (Zheng et al. 2016) and is highly correlated with mei-yu rainfall (Huang et al. 2012). An extremely early or late MWD may lead to serious drought or flood disasters. For example, the extremely late MWD in 2016 led to above-normal rainfall over the YHRB and caused economic losses of 99.31 billion CNY in China (Zhao et al. 2018), whereas the early MWD in 1994 caused massive droughts and shortages of potable water in Jiangsu and Anhui provinces in China (Chen 1995). The MWD is associated with subseasonal changes in the atmospheric circulation over East Asia, such as the East Asian jet stream (EAJS) and the western North Pacific subtropical high (WPSH) (Lin and Lu 2008; Su et al. 2017; Kuwano-Yoshida et al. 2013). The MWD also indicates the beginning of the rainy season over North and Northeast China (Ding 1992; Tao and Chen 1987) and the onset of the western North Pacific summer monsoon (Xu

Supplemental information related to this paper is available at the Journals Online website: https://doi.org/10.1175/JCLI-D-19-0768.s1.

Corresponding author: Hua Li, lihua@mail.iap.ac.cn

DOI: 10.1175/JCLI-D-19-0768.1

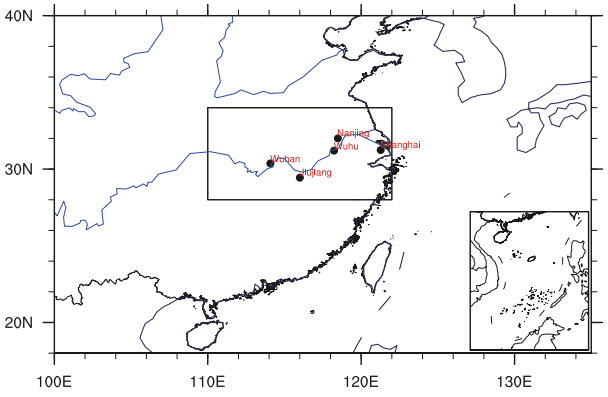

FIG. 1. The YHRB (black box) and five stations selected for calculating the MWD (black dots).

and Lu 2018). Thus studies of the MWD are important in improving short-term climate forecasting of the EASM.

The SST anomalies of various oceans have remarkable impacts on the EASM generally. Recently, much research has pointed out that the SST anomalies over North Atlantic play an important role in the East Asian and North Pacific summer climate. The SST anomalies can affect the EASM, the rainfall amount in the monsoon transitional zone of China, and the relationship between El Niño–Southern Oscillation (ENSO) and the EASM (Chen et al. 2018; Zhao et al. 2019; Zuo et al. 2019; Choi and Ahn 2019). Especially, the SST over the North Pacific has a large effect on the climate and ecosystems of the surrounding regions (Chao 1977; Matsumura et al. 2016; Sun et al. 2008; Zheng et al. 2014; Zhu et al. 2011). The extratropical SST anomalies over the North Pacific are primarily forced by the local atmosphere (Cayan 1992) but can also affect climate anomalies in East Asia (Frankignoul and Sennechael 2007; Frankignoul et al. 2011; Kwon and Deser 2007; Liu et al. 2006) and the EASM (Matsumura et al. 2016; Yu et al. 2016, 2018). In addition, Kuwano-Yoshida et al. (2013) have suggested that the SST and evaporation anomalies near the rainband of mei-yu–baiu play a vital role in maintaining the mei-yu–baiu. The Pacific decadal oscillation (PDO), the first leading mode of the SST over the extratropical North Pacific, profoundly affects the climate in the Northern Hemisphere (Mantua and Hare 2002; Mantua et al. 1997; Zhu et al. 2015). In addition, the North Pacific Gyre Oscillation (NPGO)/Victoria mode, which is the second leading mode of the SST over the extratropical North Pacific, also significantly influences the climate and ecosystems of the Pacific region (Di Lorenzo et al. 2008; Ding et al. 2015a,b). Ding et al. (2015b) showed that the Victoria mode in the boreal spring–summer affects the tropical SST over the Pacific Ocean during the following seasons through ocean–air interactions and the anomalous subsurface ocean temperature and may even develop into ENSO. Wu et al. (2006) addressed the mechanism by which the interdecadal change in the tropical Pacific SST is modulated by the interdecadal variation in the SST of the extratropical Pacific Ocean. These studies suggest that the East Asian climate is significantly influenced by SST anomalies over the extratropical North Pacific, leading to the question of whether the SST in the extratropical North Pacific can affect the mei-yu and even the MWD. First, we detected the relationship between SST in different seasons over North Pacific and MWD. In July, the SST anomalies associated with the MWD mainly located in the Kuroshio Extension and the tropical eastern Pacific (Fig. S1d in the online supplemental material). The MWD-related SST anomalies appear in the entire extratropical North Pacific in winter (Fig. S1a). Additionally, the SST anomalies' evolution from the previous winter to July partly exhibits a feature of continuity. We therefore investigated the relationship between the SST in the extratropical North Pacific in the preceding winter and the MWD and addressed the underlying mechanisms.

The North Pacific SST is characterized by multiscale variabilities from the interannual and decadal to multidecadal time scales (Jin 1997; Miller and Schneider 2000; Trenberth 1990; Yeh et al. 2011). Previous studies have found that the SST in the extratropical North Pacific showed interdecadal changes around the late 1970s and late 1980s, which induced a midlatitude climate transition on the interdecadal time scale (Deser and Phillips 2006; Xiao and Li 2007; Yeh et al. 2011). Another motivation for this study was therefore to examine whether the MWD is affected by the interdecadal change in the SST in the extratropical North Pacific.

This paper is arranged as follows. Section 2 details the datasets and methods used. Section 3 explores the recent intensified relationship between the MWD and the SST in the extratropical North Pacific. Section 4 considers the mechanisms for the impact of the extratropical North Pacific SST on mei-yu withdrawal since the early 1990s. Section 5 addresses the possible effects of the intensified interannual variability of the North Pacific SST since the early 1990s. Section 6 discusses our conclusions.

2. Datasets and methods

a. Datasets

We used global daily atmospheric reanalysis data for the time period 1961–2016 from the National Centers for Environmental Prediction–National Center for Atmospheric Research reanalysis dataset, including the specific humidity, horizontal winds, vertical velocity, geopotential height, and air temperature with a horizontal resolution of 2.5° × 2.5° and 17 vertical pressure levels (Kalnay et al. 1996). We used a gridded daily precipitation observation dataset with a horizontal resolution of 0.25° × 0.25° from >2400 observation stations in China (CN05.1) to support the results obtained from the reanalysis dataset during the time period 1961–2016 (Wu and Gao 2013). We compiled the SST during the time period 1961–2016 from the National Oceanic and Atmosphere Administration Extended Reconstructed SST V5 dataset with a resolution of 2.0° × 2.0° (Huang et al. 2017). We calculated the MWDs from a daily precipitation observational dataset from 756 stations in China during the time period 1979–2016. These data were supplied by the National Meteorological Information Center of the China Meteorological Administration.

We also used the SST from the first 30 ensemble members of the Community Earth System Model (CESM)–Large Ensemble Community Project (LENS) datasets (Kay et al. 2014). Each ensemble member in these datasets is forced by the same historical radiative fluxes for the time period 1920–2005 and with the RCP8.5

radiative fluxes for the time period 2006–2100. The first 30 members of CESM-LENS are employed in this study; those members are subject to the identical external radiative forcing but beginning from slightly different atmospheric initial conditions. We used only the time period 1961–2005 to analyze the interannual variabilities of the SST. We removed the warming trends in each member at each grid point before analyzing the CESM-LENS datasets.

b. *Definition of MWD*

We defined the MWD using the number of precipitation days from five selected stations [shown in Fig. 1; Wuhan (30°37′ N, 114°08′E), Nanjing (32°00′N, 118°48′E), Wuhu (31°20′N, 118°23′E), Jiujiang (29°44′N, 116°00′E), and Shanghai (31°24′N, 121°27′E)] and the position of the WPSH ridge (Ding et al. 2007; Li et al. 2019). We defined the MWD according to the following six criteria. 1) Rainy days were defined as when the daily precipitation at more than two of the five selected stations was >0.1 mm and the total precipitation of all five stations was >10 mm. 2) At least five rainy days occurred in the subsequent 10 days following the first rainy day. 3) The WPSH ridge was located within 20°–25°N. 4) If these three conditions were satisfied, then the first rainy day was assigned as the mei-yu onset date. 5) One or more precipitation events usually occurred during the mei-yu period and each precipitation event had more than six consecutive rainy days as defined in criterion 1, with an average rainfall for the five stations >25 mm. 6) The second day of the last precipitation event during the mei-yu period was defined as the MWD. The mei-yu period refers to these days from the mei-yu onset date to withdrawal date. Additionally, the definition of the mei-yu employed in this study originates from the definition of mei-yu of the China National Climate Center. The mei-yu definition applies to monitoring of the mei-yu in China, and it also has a wide range application in some previous studies (e.g., Li et al. 2019; Yao et al. 2019; Ding et al. 2007). Therefore, we think the five stations and the several thresholds of precipitation selected in this definition can represent the change in mei-yu to a large extent.

c. *Numerical simulations and statistical procedures*

We used the Community Atmosphere Model version 4 (CAM4) (Gent et al. 2011) to examine the impact of the SST on the MWD. CAM4 is the atmospheric component of the CESM and has finite-volume dynamics and 26 hybrid sigma–pressure levels. Section 4 details the design of the experiment. We used Student's *t* test to estimate the significance levels. We removed the linear trends for all data before analysis and used a 5-day running average for the daily datasets.

Because the mei-yu is influenced by previous winter ENSO, in this study the winter ENSO signals should be removed for all climate variables following the method of An (2003), and the following formulation is used:

$$\xi = \xi^* - Z \times \mathrm{cov}(\xi^*, Z)/\mathrm{var}(Z),$$

where ξ^* indicates the original climate variables, Z is a time series, cov means the temporal covariance between ξ^* and Z, and var means the variance. The term ξ indicates new variables, of which the signal covariants with Z are removed from ξ^*, and the ENSO variability is described by the Niño-3.4 index.

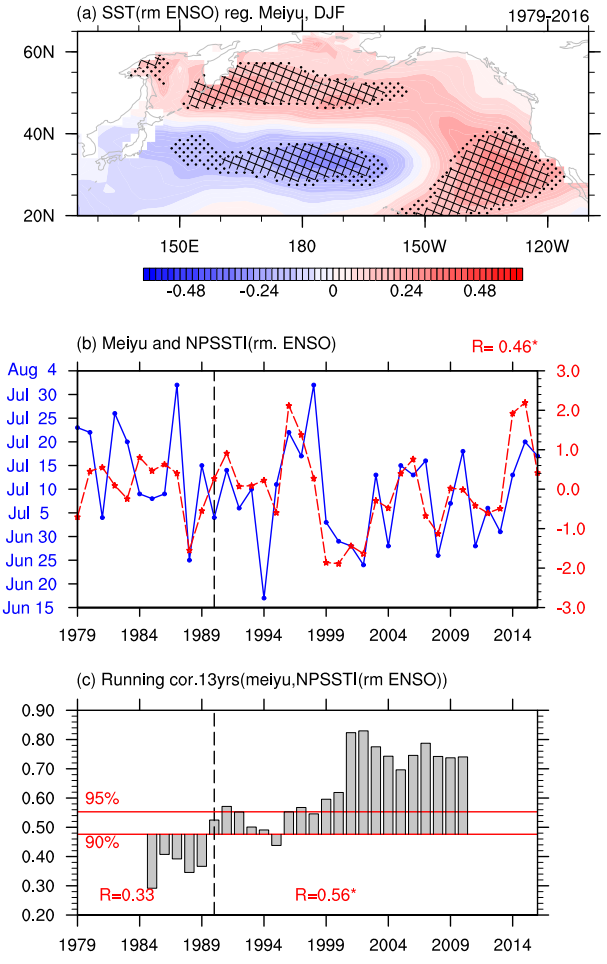

FIG. 2. (a) Regression map of the MWDs for the winter SST (unit: K) in the North Pacific. The hatched and dotted areas indicate the 95% and 90% confidence levels, respectively, based on Student's *t* test. Time series of (b) the MWDs and the NPSSTI (detrend) and (c) the 13-yr sliding correlation between MWDs and the NPSSTI. The asterisk indicates a 99% confidence level based on Student's *t* test.

3. Recent intensified relationship between the MWD and SSTs over North Pacific in winter

Statistically, the average MWD during the time period 1979–2016 occurred on 10 July and its standard deviation was 10.6 days. The earliest and latest MWD occurred in 1994 and 1998, respectively (Fig. 2b: blue curve). The large interannual variability in the MWD implies a large interannual variability of the YHRB rainfall.

To examine the relationship between the preceding winter (December–February) SST over the extratropical North Pacific and the MWD, we regressed the SST on the MWD. Figure 2a shows that the dominant SST pattern over the extratropical North Pacific related to the MWD has a horseshoe shape characterized by negative anomalous SSTs west of 150°W between 20° and 40°N and positive anomalies in the immediate surroundings. We refer to this mode as the NPSST.

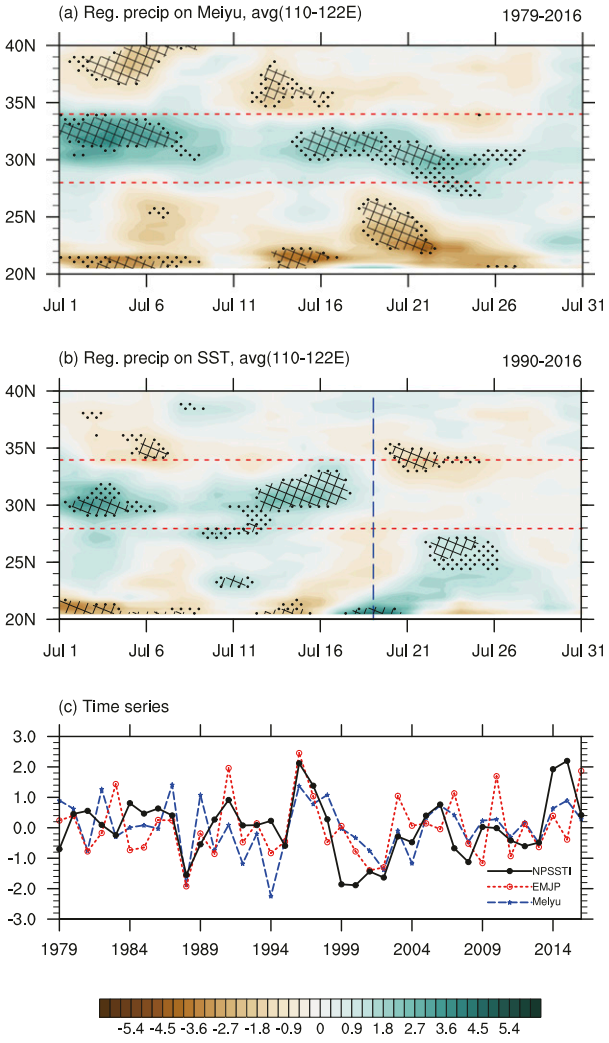

FIG. 3. (a) Regression map of the MWDs for precipitation (unit: mm day^{-1}) averaged along 110°–122°E during 1979–2016. (b) Regression map (unit: mm day^{-1}) of the NPSSTI averaged along 110°–122°E during 1990–2016. The hatched and dotted areas in (a) and (b) indicate the 95% and 90% confidence levels, respectively, based on Student's *t* test. (c) Normalized time series of the NPSSTI, the MWDs, and the EMJP.

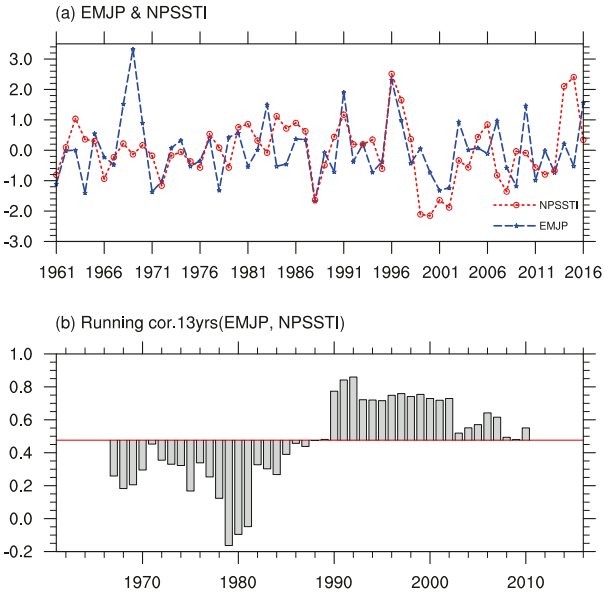

FIG. 4. Time series of (a) the normalized NPSSTI and EMJP and (b) the 13-yr sliding correlation. The red line indicates the 90% confidence level based on Student's *t* test.

The NPSST resembles the PDO (Mantua et al. 1997) and NPGO (Ding et al. 2015b) patterns, and the NPSST bears a close resemblance to those related to the Arctic Oscillation (AO) and North Pacific Oscillation (NPO) (Nakamura et al. 2006; Chen et al. 2015; Vimont et al. 2003). Here, the NPSST index (NPSSTI) was obtained by projecting the NPSST onto the SST after removing the ENSO signals (Fig. 2b, red line). The correlation coefficient between the NPSSTI and MWD was 0.46, which passed the Student's *t* test at the 0.01 significance level. The changes in the time series of the NPSSTI and MWD were more consistent after the early 1990s (Fig. 2b). We therefore used the 13-yr sliding correlation to examine the change in the relationship. Figure 2c shows that the positive correlation between the NPSSTI and MWD occurs over the whole period, with an increasingly significant relationship after the early 1990s. These results indicate that the relationship between the NPSSTI and MWD shows a clear interdecadal variability.

Previous studies have suggested that the amount of rainfall over the YHRB in July is closely related to the MWD (Huang et al. 2012; Zhao et al. 2018). To examine the covariability of the MWD and simultaneous precipitation, we conducted a temporal evolution analysis of the YHRB precipitation in July corresponding to the variations in the MWD and NPSST, respectively (Fig. 3). The corresponding precipitation based on the regression pattern with regard to the MWD during 1979–2016 spans from 1 to 25 July, whereas the significant positive precipitation anomaly based on the regression pattern with respect to the NPSSTI during 1990–2016 spans from 1 to 20 July. These results suggest that the NPSST leads to the change in the MWD by affecting precipitation between 1 and 20 July. In general, the average MWD occurs on 10 July and thus the change in the NPSST-related precipitation could effectively affect the MWD. We then defined a precipitation index using the average precipitation in early to mid-July (EMJP; from 1 to 20 July) to further examine the enhanced relationship between the NPSST and MWD since the early 1990s (Fig. 3c). The correlation coefficients between the NPSST and the EMJP during 1979–89 and 1990–2016 were 0.27 and 0.51, respectively, which corresponds with our assumption and indicates that the results are robust.

We conducted a similar analysis with the period traced back to 1961 to verify whether the enhanced relationship between the EMJP and the NPSST is valid on a longer time scale (Fig. 4a). The results obtained from the 13-yr sliding correlation indicated that the enhanced relationship between the

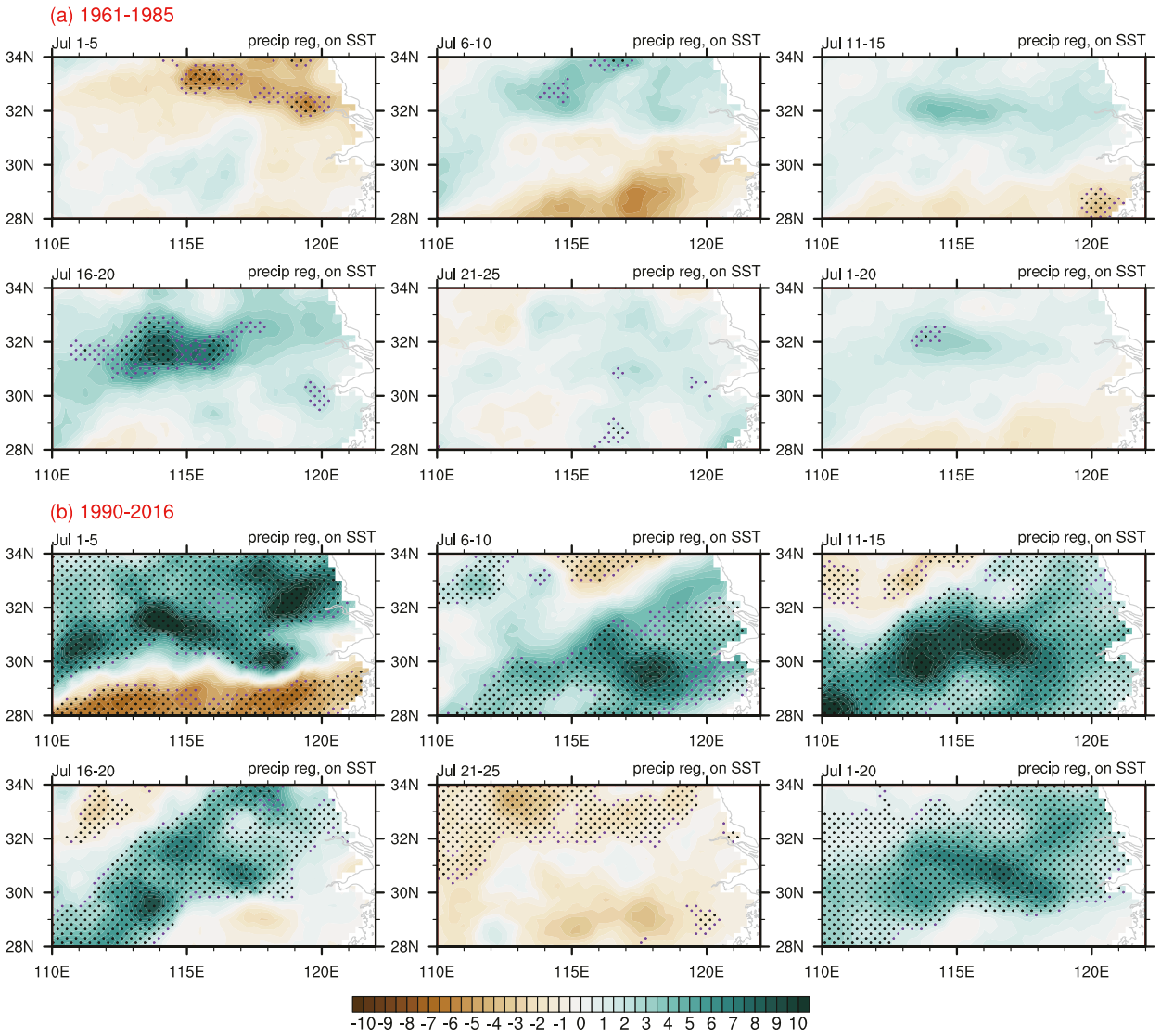

FIG. 5. Regression map on the NPSSTI for the pentad-mean precipitation (unit: mm day^{-1}) during 1–25 Jul and 1–20 Jul over the mei-yu region for (a) 1961–85 and (b) 1990–2016. The purple and black dotted areas indicate the 90% and 95% confidence levels, respectively, based on Student's *t* test.

EMJP and the NPSST (Fig. 4b) is robust and there is a significantly enhanced positive relationship from the late 1980s to the early 1990s. We therefore divided the analysis period into two periods to investigate the enhanced relationship and physical linkage between the NPSST and the MWD. We defined the first time period as from 1961 to 1985 and the second time period from 1990 to 2016.

We explored the NPSST-related anomalous pentad rainfall during 1–20 July in the first and second time periods, respectively (Fig. 5). Figure 5a shows that in the first time period the precipitation associated with the NPSST was not significant over the YHRB in the first four pentads of July, with only small-scale positive anomalies at Huaihe River (around 32°N) from 16 to 20 July. By contrast, the large-scale significant positive precipitation related to the NPSST in the second time period occurred over the YHRB during first four pentads of July and showed roughly the same features over the whole period of 1–20 July (Fig. 5b). In addition, the NPSST-related precipitation pattern from 21 to 25 July shifted to the reverse mode, with significant negative precipitation anomalies occurring over the YHRB, which implies the end of the mei-yu. We therefore suggest that the linkage between the NPSST and the MWD has strengthened since the early 1990s and has contributed to the anomalous precipitation over the YHRB from 1 to 20 July.

4. Mechanism for the significant impacts of the NPSST on the MWD since the early 1990s

The analysis in section 3 showed a significantly strengthened linkage between the NPSST and the MWD. We next

investigated the different influences of the NPSST on the atmospheric circulation and climate systems (e.g., the EAJS and WPSH) to address the possible effect of the NPSST on the MWD, and further to explore the differences between the first and second time periods to determine the factors contributing to this enhanced relationship and the physical mechanisms behind it.

The climatological southwesterly winds are prevailing over YHRB during 1–20 July in both two periods (Figs. 6a,b), which indicates the amount water vapor transported into YHRB. In the first time period, there were weak northerly anomalies associated with the NPSST in the YHRB at 850 hPa (Fig. 6c), which could impede the northward advance of the EASM and prolong the mei-yu period. The anomalous ascending motion related to the NPSST was located in the YHRB (28°–34°N), which led to a slightly above-normal rainfall (Figs. 6e and 5a). Some studies have also indicated that, as a result of the high meridional humidity gradient in the mei-yu front, the relative humidity may have an important role during the mei-yu period (Ding et al. 2007; Sun et al. 2019). We therefore also analyzed the relative humidity to examine the effects of the NPSST on the mei-yu. In the first time period, there is a weak positive anomalous relative humidity over the YHRB, which could slightly intensify the mei-yu front (Fig. 6g). The results suggest a positive and insignificant correlation between the NPSST and the MWD, in agreement with the conclusions of section 3. By contrast, in the second time period, the significant southerly anomalies dominate over the YHRB, which could transport moist air to the mei-yu rainbands (Fig. 6d). The strong and significant ascending motion related to the NPSST is located in the YHRB, which supports the above-normal rainfall (Fig. 6f) in the mei-yu period. The profound positive relative humidity anomaly associated with the NPSST suggests a strong mei-yu front (Fig. 6h). Therefore the NPSST-related atmospheric circulation anomalies support the enhanced correlation between the NPSST and the MWD.

Some studies have addressed the observation that the MWD is closely related to changes in the atmospheric circulation over East Asia on a subseasonal time scales (Dong et al. 2010; Su et al. 2017). The atmospheric circulation associated with the MWD could be changed by the WPSH and the EAJS. The NPSST-related WPSH and EAJS were therefore analyzed in the two time periods to investigate this enhanced relationship. In the first time period, the EAJS is located around 40°N and the NPSST-related zonal wind anomalies dominate over the YHRB, accompanied by weak positive geopotential height anomalies associated with NPSSTI (Figs. 7a,c). Therefore both the NPSST-related WPSH and EASJ show the causes of the weak correlation between the NPSST and the MWD. By contrast, in the second time period, the results show that intense westerly winds dominate over southern China, which leads to the southward displacement and intensification of the EAJS (Fig. 7b). Previous studies have suggested that the ascending and descending motion are generally located in the south and north, respectively, of the EAJS core (Fan et al. 2013; Lu et al. 2011). Thus, the southward displacement of the EAJS implies that the divergence at upper levels occurs over the YHRB and results in ascending motion. The NPSST-related positive geopotential height anomalies dominate over the south of South China Sea and the Philippine Sea (Fig. 7d), which leads to the westward and southward displacement of the WPSH and favors the transport of moisture to the mei-yu rainband, strengthening the mei-yu front (Li et al. 2019; Matsumura et al. 2015). These results show the NPSST could change the position and strength of the EAJS and WPSH in the second time period. The anomalous EAJS and WPSH then cause vertical motion and the transport of water vapor, respectively and, as a consequence, the MWD is changed.

We also explored how the winter NPSST can affect the MWD by changing the WPSH and EAJS after the early 1990s. Figure 8 shows the evolution of the SST and surface winds associated with the NPSST over the Pacific in different time periods. It is clear that a significant horseshoe pattern of the SST anomaly dominates over the extratropical Pacific in both time periods and the anomalous SST and surface winds over the tropical eastern Pacific show similar features to the Pacific meridional mode (PMM) (Figs. 8a,e). The PMM presents an anomalous north–south SST gradient in the tropical eastern Pacific coupled with anomalous southwesterly winds in the northeasterly trade regime (Chang et al. 2007; Chiang and Vimont 2004; Zhang et al. 2009a,b). The PMM acts as an effective conduit to influence the extratropical–tropical interaction and has a maximum variance in the winter and spring. We calculated the correlation coefficient between the NPSST and PMM index (www.esrl.noaa.gov/psd/data/timeseries/monthly/PMM/) and the results are shown in Table 1. The correlation coefficients in winter in the first and second time periods are 0.42 and 0.61, respectively. Both correlations are above the 95% confidence level, but the correlation is stronger in the second time period. The anomalous surface cyclone appears around 40°N in both the first and second time periods in winter. In the first time period, the cyclone mainly describes the features of the Aleutian low (AL), whereas in the second time period the cyclone anomaly mainly expresses the features of the southern pole of the North Pacific Oscillation (NPO) (Rogers 1981). Additionally, to examine the different relationship between NPSSTI and AL/NPO in the two time periods we calculate the correlation coefficients between them, and the AL and NPO index are defined by time series of EOF1 and EOF2 mode of winter SLP, respectively. The correlation coefficients between NPSSTI and AL (NPO) in the first and second time periods are 0.58 (0.39) and 0.08 (0.55); the results also suggest that the NPSST has a closer relationship with the NPO in the second time period. In addition, stronger southwesterly winds are located in the central to eastern tropical Pacific during the second time period than during first time period, which shows a stronger correlation between the PMM and NPSST during the second time period. The southwesterly winds warm the SSTs in situ by wind–evaporation–SST feedback (Chiang and Vimont 2004; Xie et al. 2009).

The horseshoe-shaped SST structure begins to collapse in the following spring in the first time period (Fig. 8b). By contrast, the SST mode can persistent into the following season and toward July, with a clear development of significant positive SST anomalies over the tropical regions from winter to July in the second time period (Fig. 8f). The anomalous surface

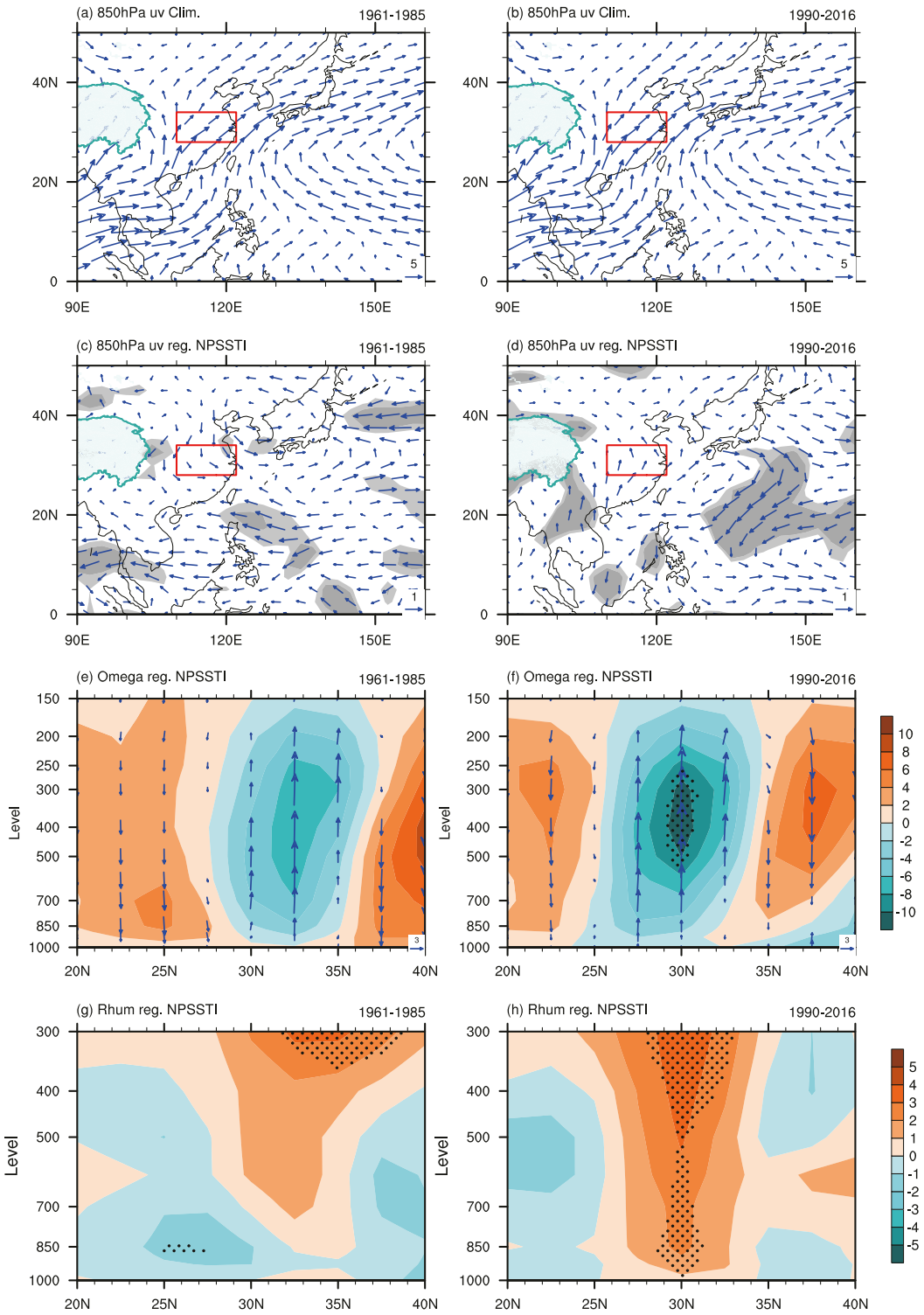

FIG. 6. The climatological distributions of wind fields (unit: m s^{-1}) at 850 hPa for 1–20 Jul during (a) the first and (b) the second time periods. The red box denotes the YHRB region. Regression map of the NPSSTI for (c),(d) the 850-hPa wind field (unit: m s^{-1}), (e),(f) omega (unit: 10^{-2} Pa s^{-1}) averaged along 110°–122°E, and (g),(h) the relative humidity (unit: %) averaged along 110°–122°E for 1–20 Jul during (c),(e),(g) 1961–1985 and (d),(f),(h) 1990–2016. The dark and light shading in (c) and (d) indicate the 90% and 95% confidence levels, respectively, based on Student's *t* test; the dotted areas in (c) and (e) indicate the 95% confidence levels based on Student's *t* test.

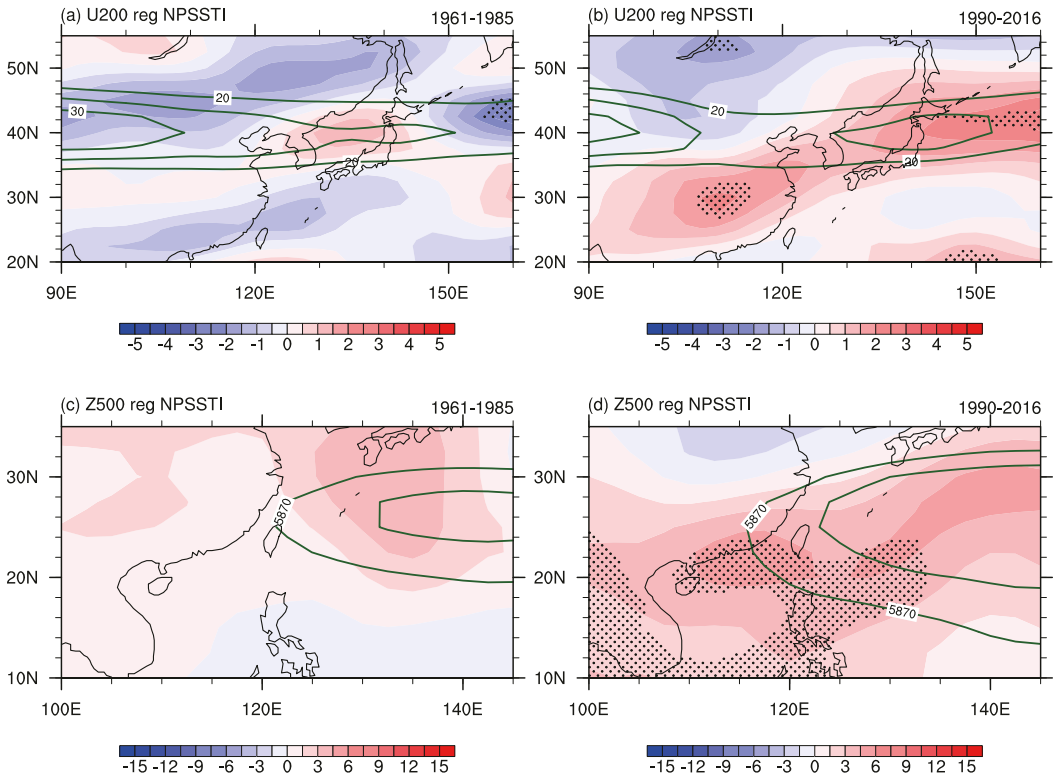

FIG. 7. Regression map on NPSSTI for (a),(b) the zonal wind at 200 hPa (unit: m s^{-1}) and (c),(d) the geopotential height at 500 hPa (unit: gpm) for 1–20 Jul during (a),(c) 1961–85 and (b),(f) 1990–2016. The dotted area indicates the 95% confidence level based on Student's t test and the contours in (a),(b) and in (c),(d) indicate the jet (>20 m s^{-1}; interval is 5 m s^{-1}) and WPSH (5880 and 5870 gpm isoclines) during their respective periods.

wind is more concentrated in the area south of 30°N than in winter (Figs. 8e,f). In particular, an anomalous cyclone appears to locate over the tropical central–western Pacific (150°E–150°W), accompanying an anomalous anticyclone over the tropical eastern Pacific (150°–90°W). The anomalous cyclone and anticyclone give rise to a warming SST over the tropical central–western Pacific, enhanced the warming anomaly. Negative SST anomalies occur over the northwestern Pacific, enhancing the zonal gradient of the SST and reinforcing the westerly anomaly over the western Pacific. Thus the enhanced westerly winds further strengthen the positive SST anomalies along the equator through air–sea interactions and a positive Bjerknes feedback process (Fig. 8g) (Bjerknes 1969). Meanwhile, previous studies have pointed out that the anomalous westerly winds over the tropical western Pacific in spring also can trigger the eastward propagating warm Kelvin waves to warm the SST in the tropical central-eastern Pacific (Huang et al. 2001; Lengaigne et al. 2004; Chen et al. 2014). The NPSST-related SST and surface wind anomalies show a more significant PMM pattern, which may be a crucial factor in enhancing the tropical Pacific SST anomaly in June. Consequently, the positive SST anomalies over the tropical Pacific can persist into July, which resembles the process revealed by Ding et al. (2015b) in which the Victoria mode affects the ENSO. We use the Niño-3.4 index to represent the SST anomaly over the central–eastern Pacific and then calculate the correlation coefficient between the NPSST in winter and the Niño-3.4 index in June and July. The results show that a high correlation occurs in the second time period and the correlation coefficients in June and July are above the 95% confidence level (Table 1). The results also imply that the NPSST could affect the SST over the central–eastern Pacific in the second time period. The NPSST-related SST over the ocean east of Japan also appears to be clearly different between the first and second time periods; there are larger and stronger negative SST anomalies in the second time period than in the first time period (Figs. 8d,f).

Yu et al. (2018) reported that the positive SST anomalies over the ocean east of Japan could have led to less precipitation in the Yangtze River basin in summer since 1990 by changing the meridional temperature gradient. Previous studies also suggested that the summer WPSH could be affected by the tropical Pacific SST after the early to mid-1990s (He and Zhou 2015; Wu and Wang 2019; Yun et al. 2010). Therefore the anomalous SST in July over the throughout the North Pacific induced by the NPSST has a key influence on the variations in the WPSH and EAJS from 1 to 20 July, which, in turn, affects the MWD.

Moreover, in this part, we also explore how the NPSST-related SST anomalous in July cause the anomalies of EAJS and WPSH during the second time period. The EAJS anomalies are mainly affected by the distribution of temperature

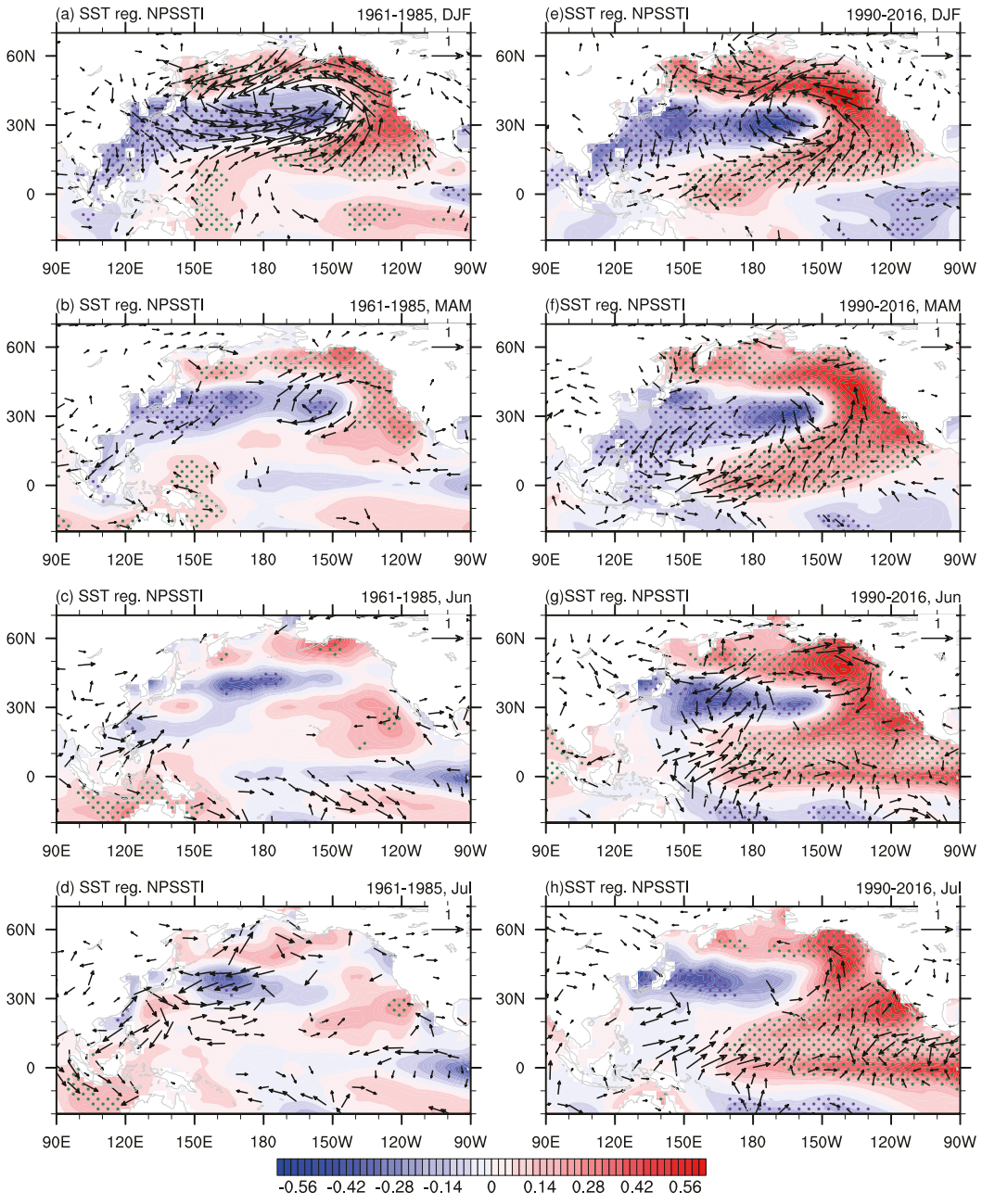

FIG. 8. (a)–(d) Regression map of the SST (colors; the dotted area indicates the 95% confidence level based on Student's *t* test) and surface wind field (vectors; only those >90% confidence level are plotted) in winter, spring, June, and July, respectively, during 1961–85. (e)–(h) Regression map of the SST (colors; the dotted area indicates the 95% confidence level based on Student's *t* test) and surface wind field (vectors; only those >90% confidence level are plotted) in winter, spring, June, and July, respectively, during 1990–2016.

anomalies, especially the meridional temperature gradient, at middle to upper levels of the troposphere. Thus, we examine the NPSST-related anomalous temperature and meridional temperature gradient anomalies at middle to upper levels (mass-weighted average from 500 to 200 hPa) in the second time period; notably, we multiply the temperature gradient anomalies by a minus sign for more vivid descriptions of results (Figs. 9a,b). The positive and negative temperature anomalies are located in the central-eastern Pacific and near Northeast Asia, respectively. The NPSST-related air temperature anomalies roughly correspond to the NPSST-related SST anomalies in July (Fig. 8h), but the air temperature is tilted to the northwest. Those distributions of temperature anomalies give rise to a stronger minus meridional temperature gradient

TABLE 1. Correlation coefficients between the NPSSTI and different indexes in the two time periods. One asterisk (*) indicates >95% confidence level, and two asterisks (**) indicate >99% confidence level, based on Student's *t* test.

	PMM_ winter	PMM_ spring	Niño-3.4_June	Niño-3.4_July
NPSSTI_pre	0.42*	0.17	−0.16	−0.03
NPSSTI_post	0.61**	0.67**	0.58**	0.46*

around 30°N over East Asia, which implies the southward displacement and intensification of EAJS. In addition, the vertical motion and heating source play a vital role in the position and strength of the WPSH (Wang et al. 2006, 2011; Li et al. 2019). The anomalous upwelling and downwelling motion in the second time period associated with the NPSST locate around 10° and 20°N over the western Pacific (Figs. 9c,e), roughly matching the positive and negative SST anomalies over western Pacific associated with the NPSST in July, respectively (Fig. 8h). The downwelling motion around 20°N over western North Pacific results in the southward displacement of the WPSH. Meanwhile, apparent NPSST-related atmospheric heating anomalies, which are calculated based on Yanai et al. (1973), describe a negative anomaly around the 20°N over western North Pacific (Fig. 9d). The negative anomalies of atmospheric apparent heating favor a southward-shifting WPSH (Wang et al. 2006). Notably, the atmospheric apparent heating anomalies coincide well with the anomalous vertical motion. Thus, the EASJ and WPSH during 1–20 July are caused by NPSST-related SST anomalies in July via changing air temperature and vertical motion associated with the NPSST in the second time period.

Furthermore, we used numerical simulations to verify this mechanism that the anomalous SST in July associated with NPSST impacts the EASJ and WPSH, ultimately influencing the mei-yu. We employ the CAM4 and design two experiments as follows. The first experiment is 50 years of integration forced with the climatological SST and sea ice boundary conditions, defined as the control run (Ctrl); the second experiment is the same as the first, but the anomalous SST shown in Fig. 10a is

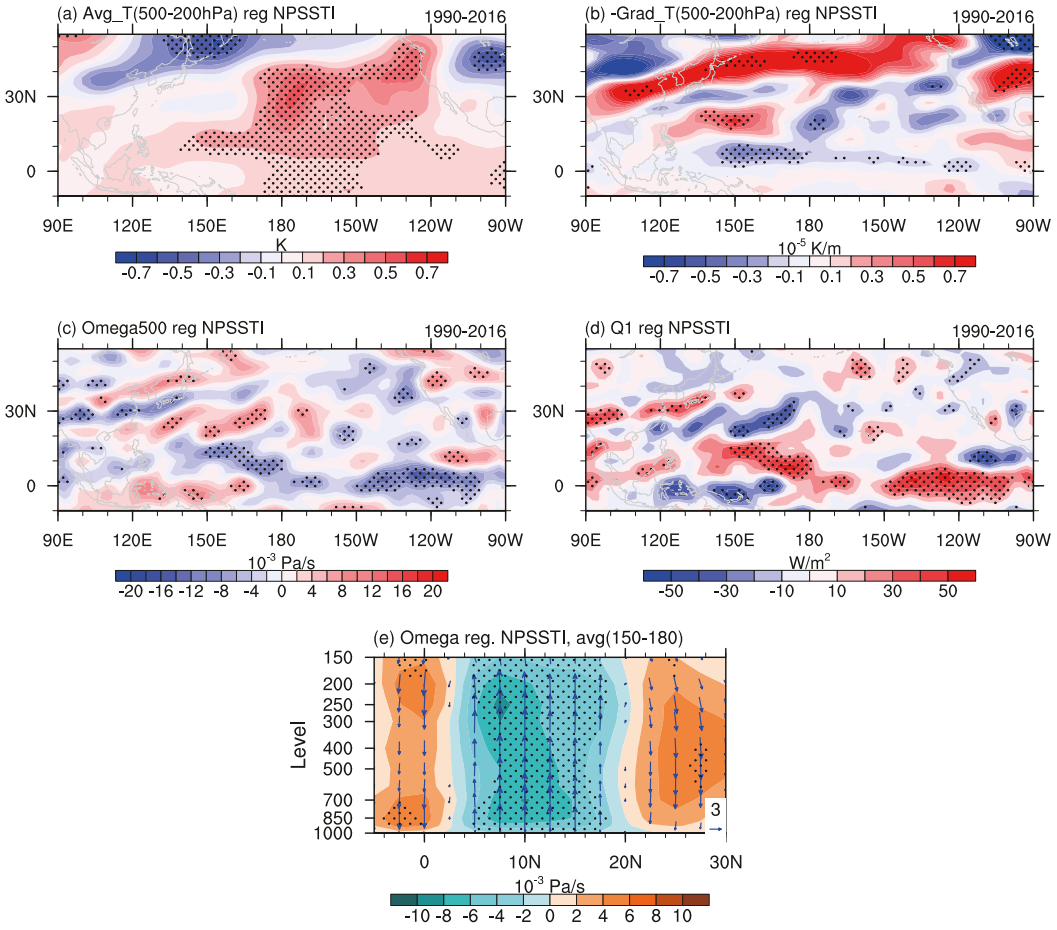

FIG. 9. Regression map of mass-weighted average (a) temperature and (b) minus the meridional temperature gradient from 500 to 200 hPa during 1–20 Jul onto NPSSTI in the period 1990–2016. Regression map of (c) omega at 500 hPa, (d) atmospheric apparent heating (Q_1), and (e) omega averaged along 150°E–180° during 1–20 Jul onto NPSSTI in the period 1990–2016. The dotted areas indicate the 90% confidence level based on the Student's *t* test.

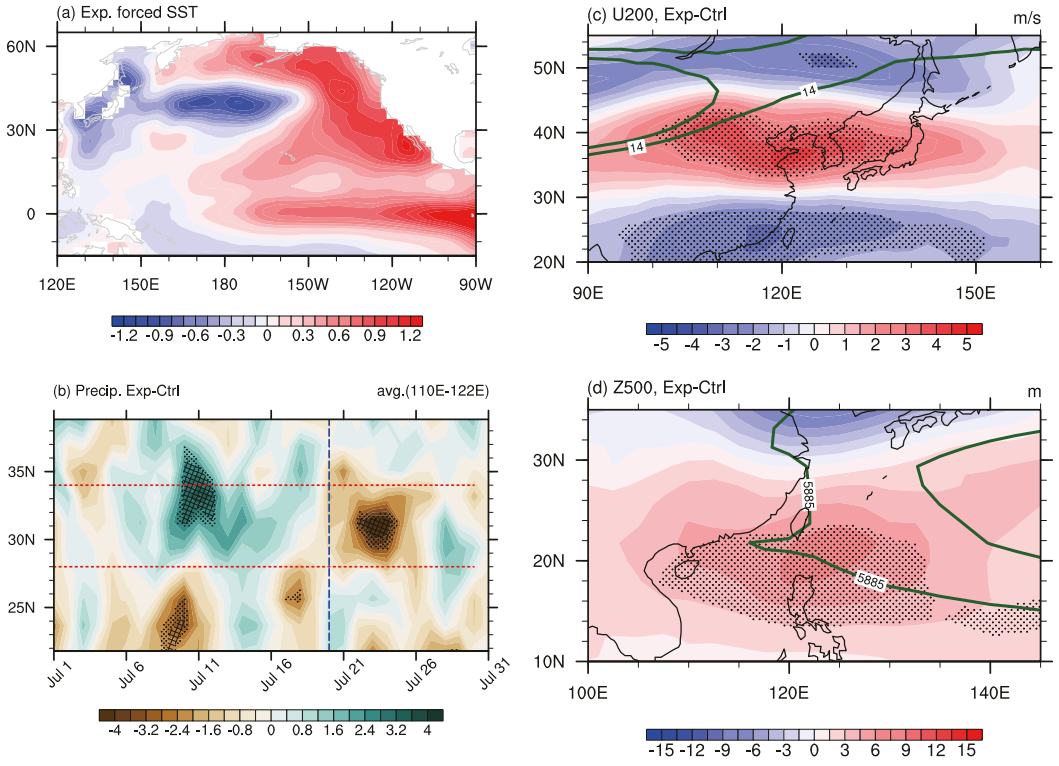

FIG. 10. (a) Forced SST anomaly in July in the sensitivity experiment relative to the control experiment, (b) the difference in precipitation averaged along 110°–122°E between the sensitivity and control experiments, and the difference in the (c) zonal wind at 200 hPa and (d) the geopotential height at 500 hPa between the sensitivity and control experiments during 1–20 Jul. The dotted areas indicate the 90% confidence level based on Student's *t* test. The contours in (c) and (d) indicate the jet stream and the WPSH during 1–20 Jul in the control experiment.

added as the July SST (defined as the sensitivity experiment, Exp). The anomalous SST in July is obtained by the composited SST anomaly of the years exceeding one standard deviation of the NPSSTI during 1990–2016. The first 20 years are used for the model spinup and the last 30 years are used for analysis. It should be noted that the 30-yr mean values are equivalent to the values from an ensemble of 30 samples created by different initial atmospheric and land surface conditions.

Figure 10b shows the precipitation averaged along 110°–122°E in July for the two experiments. It is clear that positive precipitation anomalies dominate in the YHRB and the maximum positive value center occurs around 11 July, which supports the above-normal precipitation and later MWD in the sensitivity experiment. To compare the differences between the EAJS and WPSH in the two experiments, we analyze the zonal wind at 200 hPa and the geopotential height at 500 hPa between the sensitivity and control runs (Figs. 10c,d). As a result of the systematic errors in the model, there are some differences in the climate systems (the EASJ and WPSH) between the control run and the real atmosphere. Compared with the observed datasets, the EASJ in the control run is weaker and in a more northward position, whereas the WPSH is stronger in the control run. The composite analysis of the zonal wind at 200 hPa between the control and sensitivity runs shows that the significant intensified westerly winds dominate around 35°N (colors in Fig. 10c) and the maximum zonal wind is located north of 40°N (green lines in Fig. 10c). These results imply that the strengthened and displaced southward EAJS is expressed more in the sensitivity experiment than in the control run. The composite analysis of the geopotential height at 500 hPa shows the significant areas of high pressure located in the south of the South China Sea and the Philippine Sea (colors in Fig. 10d). These results suggest that the intensified and displaced westward and southward WPSH can be seen in the sensitivity experiment. These results from numerical experiments confirm the observational results. Therefore both the numerical results and the observations support the conclusion that the NPSST-related SST over the Pacific in July can exert great a large effect on the MWD by modulating the WPSH and EAJS in the second time period.

5. Possible mechanism for the enhanced persistent SST anomaly over the North Pacific after the early 1990s

This section discusses the possible mechanism for the more persistent SST anomalies associated with the NPSST during the second time period. The NPSST mode is similar to the pattern of the PDO and NPGO. To explore the relationship between the NPSST and PDO/NPGO, we use the empirical orthogonal function (EOF) to analyze the winter SST (the

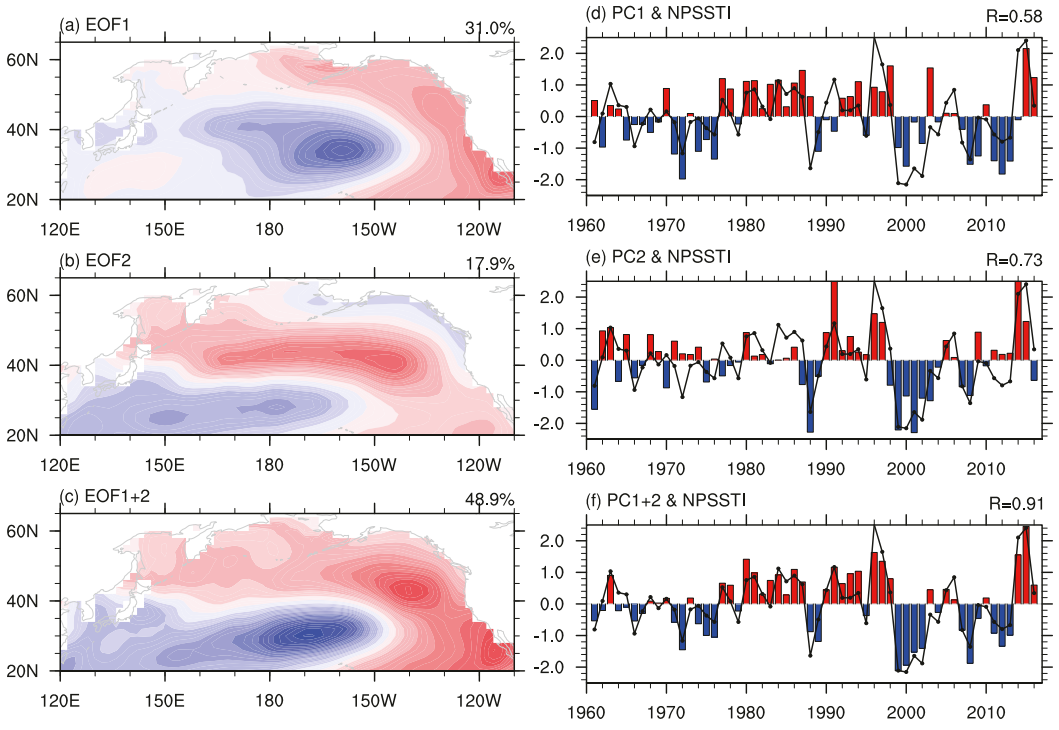

FIG. 11. The EOF mode of the winter North Pacific SST during 1961–2016: (a),(b) EOF1 and EOF2, respectively; (d),(e) the time series of EOF1 and EOF2, respectively, (c) the combined mode of EOF1 and EOF2, and (f) the time series of the combined mode. The black lines in (d)–(f) indicate the NPSSTI.

signals of ENSO have not been removed) over the North Pacific during 1961–2016. Figure 11 shows the spatial distribution of the leading two modes and the corresponding time series. The first two leading modes are independent of each other and are statistically distinguished from the other modes according to the rule given by North et al. (1982). The first and second leading modes present a PDO-like mode and a NPGO-like mode, respectively, which explain 31% and 17.9%, respectively, of the variance of the variability in the SST over the North Pacific. Figures 11d and 11e show the time series of the PDO-like and NPGO-like mode indexes, respectively, and both PDO-like and NPGO-like modes show clear interannual to interdecadal variabilities. Because the NPSST has similar spatial features to the PDO-like and NPGO-like modes, we calculate the spatial and temporal correlation coefficient between the NPSST and PDO-like/NPGO-like modes. The spatial (temporal) correlation coefficient between the NPSST and the PDO-like mode is 0.43 (0.58) and the spatial (temporal) correlation coefficient between the NPSST and the NPGO-like mode is 0.68 (0.73), with all correlation coefficients above the 99% confidence level. We directly sum the distributions of the PDO-like and NPGO-like modes due to their independence (Fig. 11c). Similarly, we also sum the time series of the PDO-like and NPGO-like modes (Fig. 11f). The pattern correlation coefficient between the new mode (PDO-like + NPGO-like) and the NPSST is 0.78 and their temporal correlation coefficient is 0.91.

Similarly, Zhang et al. (2018) used the combined EOF leading modes to explore the relationship between stratospheric ozone loss and the polar vortex, so the method that we use to combine the PDO-like and NPGO-like modes is reliable. When we remove the linear ENSO signals from the SST, the pattern and time correlations between the NPSST and the combined mode of EOF1 are up to 0.88 and 0.95, respectively. However, the EOF1 and EOF2 are not independent of each other, so we keep the linear ENSO signals; the results are robust with or without the ENSO linear signals. We therefore conclude that the NPSST mode is caused by a combination of PDO-like and NPGO-like modes.

Previous studies have suggested that the decadal change in the interannual variability of the SST could cause the decadal change in the influence of the SST. Ding et al. (2015b) suggest that the interannual variability of the Victoria mode determines the linkage between the Victoria mode and the ENSO. When the Victoria mode has a pronounced interannual variability, its impact on the ENSO is stable and vice versa. Yeh et al. (2011) showed that the interdecadal change in the climate over the North Pacific is dominated by the interdecadal change in the interannual variability of the PDO-like and NPGO-like modes. Therefore we examined the interannual variabilities of the NPSST, PDO-like, and NPGO-like modes by conducting a 15-yr running-variance analysis. The interannual variability of the PDO-like mode is stronger before the early 1980s and decreases after the early 1980s, then recovers significantly after the early and mid-1990s (blue line in Fig. 12). By contrast, the interannual variability of the NPGO-like mode is smaller before the mid-1980s and rapidly increases after the mid- and late

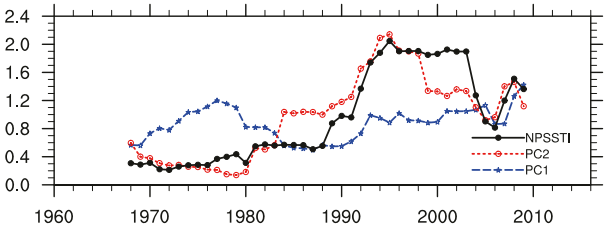

FIG. 12. The 15-yr sliding variances of the NPSSTI, PC1, and PC2.

1980s. The changes in the interannual variabilities of the PDO-like and NPGO-like modes are consistent with previous studies (Bond et al. 2003; Ding et al. 2015b; Yeh et al. 2011). The changes in the interannual variabilities of both the PDO-like and NPGO-like modes lead to a stronger interannual variability of the NPSST since the early 1990s. Therefore the strong interannual variability may have a crucial role in the recently enhanced relationship between the NPSST and the MWD during the second time period.

To explore the effects of the NPSST, PDO-like, and NPGO-like modes with different interannual variabilities, we analyzed the sea level pressure (SLP) and surface winds in winter associated with these three indexes in the two time periods. In the first time period, the anomalous SLP fields related to the NPSST present a monopole (Aleutian low) pattern, with surface wind anomalies dominant north of 20°N. By contrast, the anomalous SLP fields in the second time period show a dipole mode (the NPO) and the anomalous surface wind extends south of 20°N, which enhances air–ocean interactions and leads to more persistent SST anomalies (Figs. 13a,b). With respect to the atmospheric circulation anomalies related to the PDO-like pattern, the SLP and surface wind anomalies resemble the NPSST-related pattern in the first time period (Fig. 13c). In the second time period, however, the SLP fields also present a monopole mode, but this seems to move more eastward and

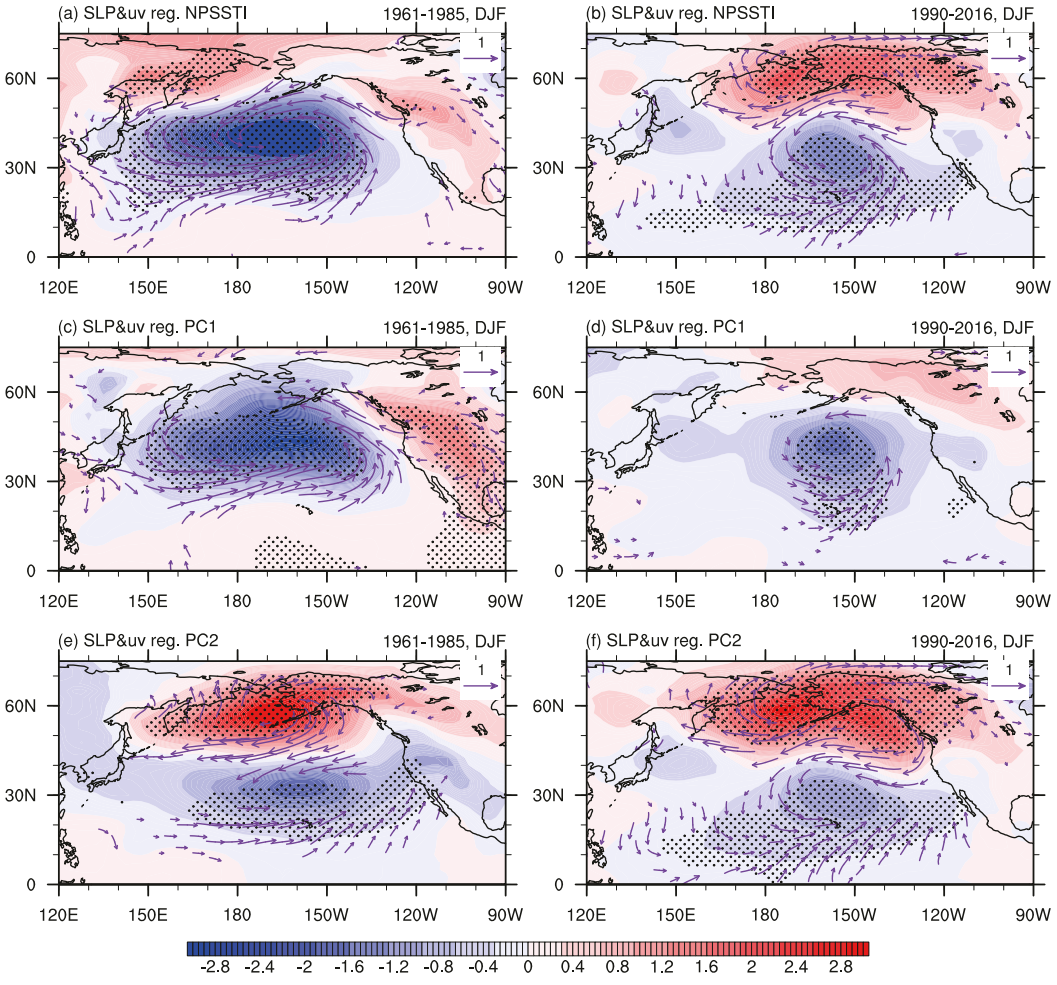

FIG. 13. The (a) NPSSTI-, (c) PC1-, and (e) PC2-related SLP (colors; the dotted area indicates the 95% confidence level based on Student's *t* test) and surface winds (vectors; only those >95% confidence level are plotted) during 1961–85. The (b) NPSSTI-, (d) PC1-, and (f) PC2-related SLP (colors; the dotted area indicates the 95% confidence level based on Student's *t* test) and surface winds (vectors; only those >95% confidence level are plotted) during 1990–2016.

southward, which resembles the southern pole of the NPO (Fig. 13d). Subsequently, the anomalous surface winds extend to the south of 20°N during the second time period. In both the first and second time periods, the NPGO-like related SLP anomaly resembles the NPO. However, the anomalous NPO pattern in the second time period has a greater amplification and its position is more southward than that in the first time period (Figs. 13e,f). The anomalous NPO pattern with a greater amplification and more southward position may have a close relationship with enhanced interannual variability of the NPGO-like mode in the second time period. Figures 13d and 13f show that the PDO- and NPGO-like related anomalous SLP and winds are similar to each other south of 50°N in the second time period.

The NPSST, as the combined mode of the PDO- and NPGO-like modes and the signals of the PDO- and NPGO-like related anomalies, may strengthen the NPSST-related southern pole of the anomalous NPO pattern. The intensity of the NPSST-related anomalous SLP is about −2 hPa, which is greater than that of the PDO- and NPGO-like related anomalous. Previous studies have found that the southern pole of the NPO modulates the influence of the extratropical circulation on tropical regions (Di Lorenzo et al. 2010; Furtado et al. 2012; Xie et al. 2019; Yu et al. 2018). Additionally, in order to examine the effects of PDO-like and NPGO-like mode on the SST anomalies, the evolution of SST anomalies associated with the PC1 and PC2 are analyzed, respectively. The results are similar to the NPSST-related results, the SST anomalies are more significant and persistent in second time period (not shown). Therefore the strong interannual variabilities of both the PDO- and NPGO-like modes lead to the intensified interannual variability of the NPSST and result in an enhanced southern pole of the NPO, a more persistent SST anomaly and, ultimately, the anomalous SST in July affects the MWD.

Furtherly, we use the SST of first 30-member model results from CESM-LENS datasets during 1961–2005. First, we obtain the NPSSTI of the model through the projection of the NPSST mode to the all SSTs (30 members × 45 years) in all individual members of CESM-LENS. We then investigate whether the NPSST is a combined mode of first two leading modes in the model. Figures 14a–c show the spatial distribution of first two leading modes of the model's SST, which suggest that the NPSST mode could also be a result of the combination of the first two leading modes of the SST over the North Pacific based on the model simulations. The scatterplots of time series of leading modes versus NPSSTI in model also suggest that the NPSST mode is a combination of the PDO- and NPGO-like modes. Thus, the results revealed by the CESM-LENS dataset indicate that the results of the observations are robust. Meanwhile, we also conduct the EOF using ensemble-mean SST of CESM-LENS for confirming the robustness of the NPSST mode; the results are similar to results revealed by ensemble-mean SST (Fig. S2). The results suggest that the external forcing from the climate system also could influence the PDO-like, NPGO-like, and NPSST modes. More explanations about the results revealed by CESM-LENS will be discussed in the next section.

6. Conclusions and discussion

The mei-yu is an important component of the EASM and its variability and evolution have an essential role in the distribution of rainbands over East Asia (Li and Zhang 2014). The MWD signals the end of the monsoon rainy season over the YHRB and the start of the rainy season over North and Northeast China (Tao and Chen 1987). The MWD has a large interannual variability and is therefore difficult to forecast. Because the North Pacific SST has important effects on the climate over the Pacific Ocean and nearby areas, we explored the relationship between the MWD and the SST over the North Pacific in the preceding winter to unravel the mechanism of the interannual to interdecadal variability of the MWD.

The MWD-related SST anomaly over the extratropical North Pacific in winter (the NPSST) shows a horseshoe mode, with positive anomalous SSTs west of 150°W between 20° and 40°N and negative anomalies over the surroundings. The NPSST is a combined mode of PDO-like and NPGO-like modes, as confirmed in both the observed and modeled SSTs. The correlation coefficient between the NPSSTI and the MWD is 0.46 and a sliding correlation shows that the significant linkage between the NPSST and MWD has increased since the early 1990s. In addition, the NPSST-related anomalous precipitation over the YHRB spans from 1 to 20 July after the early 1990s, which suggests that the NPSST affects the MWD through the anomalous precipitation in this time period. The enhanced relationship between the NPSST and the MWD is confirmed in long-term observation datasets by the precipitation index over the YHRB from 1 to 20 July. We therefore divided the study period into two periods (1961–85 and 1990–2016) to address the enhanced relationship between the NPSST and the MWD.

In the second time period, the NPSST-related circulation, vertical motion, and relative humidity anomalies on 1–20 July describe significant signals and could directly change the MWD. By contrast, the NPSST-related anomalies do not show significant signals in the first time period. The NPSST-related climate systems support the suggestion that the NPSST affects the circulation, vertical motion, and relative humidity by changing the intensities and positions of the WPSH and EAJS in the second time period. In general, a positive NPSST corresponds to an intensified and displaced southward displaced EAJS and an intensified and southward and westward displaced WPSH on 1–20 July. This results in ascending motion over the YHRB and strengthens the mei-yu front, leading to a delay in MWD and vice versa. However, the NPSST-related anomalies of the WPSH and EAJS are negligible in the first time period, thus the NPSST does not have a significant effect on the MWD during the first time period. We also analyzed the evolution of the SST associated with the NPSST in the two time periods and the results show that, compared with the first time period, the SST anomalies associated with the NPSST are more sustainable and could affect the SST over the tropical Pacific Ocean in the following months in the second time period. The anomalous SST over the North Pacific in July then changes the WPSH and EAJS via anomalous air temperature at middle to upper levels of troposphere and vertical motion and, as a

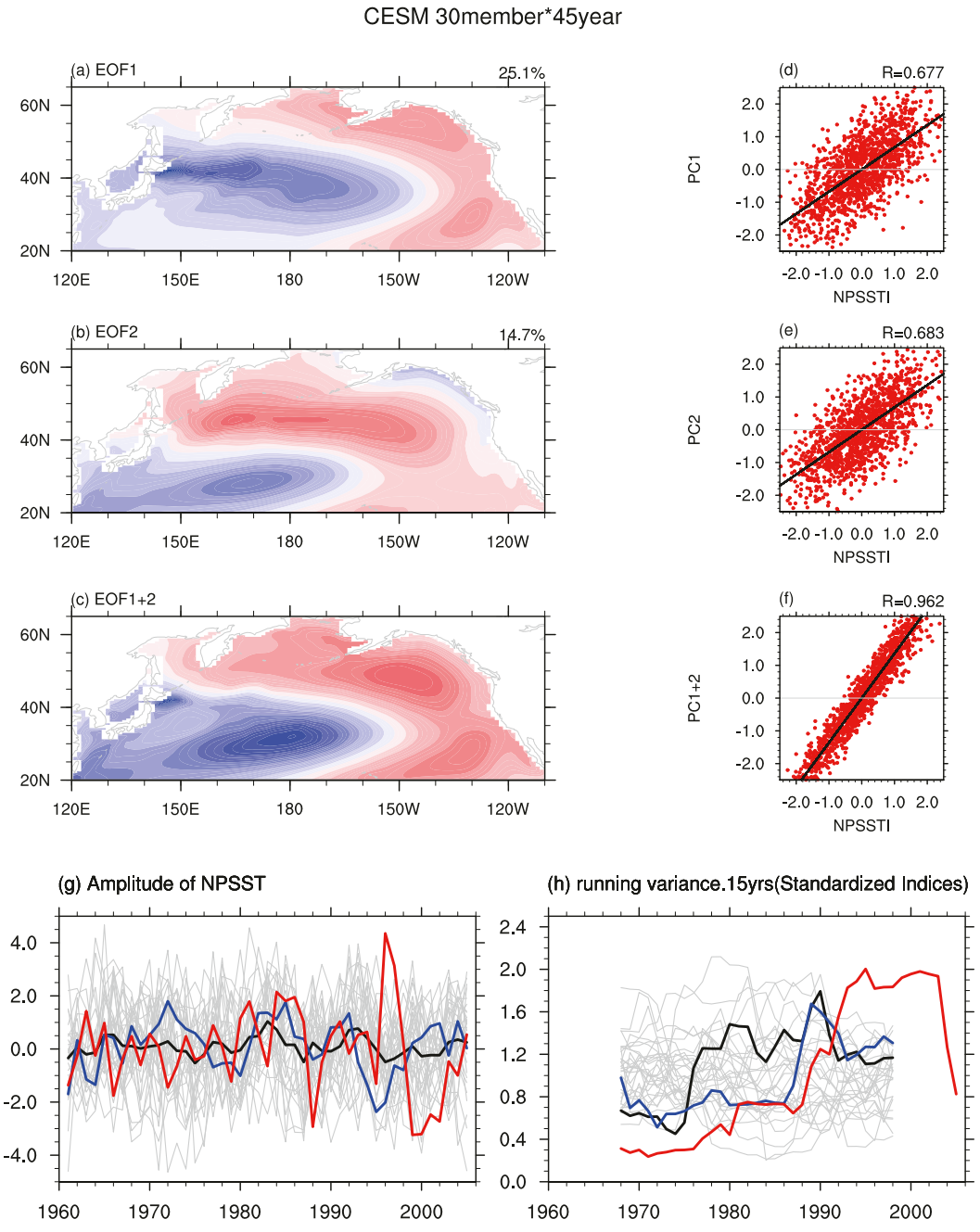

FIG. 14. The EOF modes of the winter North Pacific SST obtained from the first 30 members of the CESM-LENS dataset during 1961–2005 (30 members × 45 years) and the scatterplot of time series in EOF modes vs NPSSTI. (a),(b) The EOF1 and EOF2 mode, respectively. (d),(e) The time series of EOF1 and EOF2 vs NPSSTI, respectively. (c) The combined mode of EOF1 and EOF2. (f) The time series of the combined mode of EOF1 and EOF2 vs NPSSTI. The abscissa and ordinate in (d)–(f) denote the NPSSTI and time series, respectively. The black lines in (d)–(f) denote the regression line upon NPSSTI. (g) The raw indices of NPSST mode from all 30 members (gray curves), the ensemble-mean SST (black curve), the mean of the four members that match the observations (blue curve), and the NPSST in observation (red curve). (h) As in (g), but for the 15-yr sliding variance of normalized time series.

consequence, affects the MWD. This result is confirmed using an atmospheric general circulation model.

We also explored the possible mechanisms in the different processes of the evolution of the SST in the first and second time periods. The running variances of the NPSST, PDO-like, and NPGO-like modes show that the PDO-like and NPGO-like modes have greater interannual variabilities in the second time period and give rise to an NPSST with a greater

interannual variability in this period. The NPSST-related SLP shows significant NPO-like anomalies, especially the southern pole of the NPO with a larger amplitude and more southward location. The anomalous NPO (mainly the southern pole of the NPO) enhances the impact of the extratropical and tropical regions. The NPSST-related SST anomaly persists to July and leads to an anomalous SST over the tropical Pacific Ocean.

The PDO-like and NPGO-like modes show greater interannual variabilities in recent decades, when the greater interannual variabilities of the leading mode of the SST lead to a strengthened effect of the extratropical SST in winter on the climate over East Asia during following months. Our observations show that there is a significantly enhanced interannual variability of the NPSST. Meanwhile, the results from CESM-LENS also confirm the NPSST mode is combination mode of PDO- and NPGO- like modes. Thus, in this section, we will discuss the possible mechanism of the enhanced interannual variabilities of NPSST mode using the CESM-LENS datasets. It can be assumed that the spreads of the intermember and ensemble means indicate the internal climate variability and external forcing, respectively (Deser et al. 2016). As shown in Fig. 14g, the contribution of atmospheric internal variability to the amplitude of NPSST variance is larger than the externally forced one (Fig. 14g, gray curves vs black curve). However, only four individual members have shown an increasing of interannual variability (Fig. 14h, blue curves). On the other hand, the interannual variability of forced-NPSST mode has also shown a similar increasing trend as the observation (Fig. 14h). Therefore, it is implied that the observed increase of interannual variability of the NPSST could be induced by both atmospheric internal variability and external forcing, while the amplitude of the increase depends on the internal variability. We acknowledge that such conclusions should be further confirmed by multimodel simulations in future.

Furthermore, Joh and Di Lorenzo (2017) reported that the NPGO and PDO have shown increased coupling in recent decades, which has led to marine heatwaves in the northeast Pacific. They further investigated the future trend of the coupling relationship between the NPGO and the PDO and showed this to be very robust in the model projection for 2100 under the RCP8.5 scenario. Our study shows that the coupling and interannual variabilities of the PDO and NPGO have an important effect on the climate and ecosystem over the Pacific Ocean and the nearby areas. Further work is required to consider how the interannual variabilities of the dominant modes of the North Pacific will change in the future and how the relationship between the North Pacific SST and the mei-yu (even the climate over East Asia) will be affected by the global climate change. On the other hands, the key effects of NPO anomalies induced by the strengthened interannual variabilities SST on the enhanced relationship between the NPSST and MWD are emphasized in this study. Meanwhile, previous studies have suggested that the Atlantic multidecadal oscillation (AMO) exert remarkable influences on the PDO and climate over the Pacific region, and can also modulate the relationship between the NPO and SST anomalies over the Pacific (McGregor et al. 2014; Li et al. 2016; Chen et al. 2019). Thus, the AMO might partly modulate the relationship between the NPSST and MWD, and the hypothesis should also be addressed in the future.

Acknowledgments. This research was supported by the National Key Research and Development Program of China (Grant 2016YFA0600703) and the National Natural Science Foundation of China (Grants 41875118).

REFERENCES

An, S., 2003: Conditional maximum covariance analysis and its application to the tropical Indian Ocean SST and surface wind stress anomalies. *J. Climate*, **16**, 2932–2938, https://doi.org/10.1175/1520-0442(2003)016<2932:CMCAAI>2.0.CO;2.

Bjerknes, J., 1969: Atmospheric teleconnections from the equatorial Pacific. *Mon. Wea. Rev.*, **97**, 163–172, https://doi.org/10.1175/1520-0493(1969)097<0163:ATFTEP>2.3.CO;2.

Bond, N. A., J. E. Overland, M. Spillane, and P. Stabeno, 2003: Recent shifts in the state of the North Pacific. *Geophys. Res. Lett.*, **30**, 2183, https://doi.org/10.1029/2003GL018597.

Cayan, D. R., 1992: Latent and sensible heat flux anomalies over the northern oceans: The connection to monthly atmospheric circulation. *J. Climate*, **5**, 354–369, https://doi.org/10.1175/1520-0442(1992)005<0354:LASHFA>2.0.CO;2.

Chang, P., and Coauthors, 2007: Pacific meridional mode and El Niño–Southern Oscillation. *Geophys. Res. Lett.*, **34**, L16608, https://doi.org/10.1029/2007GL030302.

Chao, J., 1977: On the large-scale interactions of sea and atmosphere and long-range weather forecasts. *Chin. J. Atmos. Sci.*, **1**, 223–233.

Chen, S., B. Yu, and W. Chen, 2014: An analysis on the physical process of the influence of AO on ENSO. *Climate Dyn.*, **42**, 973–989, https://doi.org/10.1007/s00382-012-1654-z.

——, ——, and ——, 2015: An interdecadal change in the influence of the spring Arctic Oscillation on the subsequent ENSO around the early 1970s. *Climate Dyn.*, **44**, 1109–1126, https://doi.org/10.1007/s00382-014-2152-2.

——, R. Wu, and W. Chen, 2018: Modulation of spring northern tropical Atlantic sea surface temperature on the El Niño–Southern Oscillation–East Asian summer monsoon connection. *Int. J. Climatol.*, **38**, 5020–5029, https://doi.org/10.1002/joc.5710.

——, L. Song, and W. Chen, 2019: Interdecadal modulation of AMO on the winter North Pacific Oscillation–following winter ENSO relationship. *Adv. Atmos. Sci.*, **36**, 1393–1403, https://doi.org/10.1007/s00376-019-9090-1.

Chen, Y., 1995: The features of weather/climate in China in 1994 (in Chinese). *Meteor. Mon.*, **21**, 22–24.

Chiang, J. C. H., and D. J. Vimont, 2004: Analogous Pacific and Atlantic meridional modes of tropical atmosphere–ocean variability. *J. Climate*, **17**, 4143–4158, https://doi.org/10.1175/JCLI4953.1.

Choi, J. W., H. D. Kim, and B. Wang, 2019: Interdecadal variation of Changma (Korean summer monsoon rainy season) retreat date in Korea. *Int. J. Climatol.*, **40**, 1348–1360, https://doi.org/10.1002/joc.6272.

Choi, Y., and J. Ahn, 2019: Possible mechanisms for the coupling between late spring sea surface temperature anomalies over tropical Atlantic and East Asian summer monsoon. *Climate Dyn.*, **53**, 6995–7009, https://doi.org/10.1007/s00382-019-04970-3.

Deser, C., and A. S. Phillips, 2006: Simulation of the 1976/77 climate transition over the North Pacific: Sensitivity to tropical

forcing. *J. Climate*, **19**, 6170–6180, https://doi.org/10.1175/JCLI3963.1.

——, L. Terray, and A. S. Phillips, 2016: Forced and internal components of winter air temperature trends over North America during the past 50 years: Mechanisms and implications. *J. Climate*, **29**, 2237–2258, https://doi.org/10.1175/JCLI-D-15-0304.1.

Di Lorenzo, E., and Coauthors, 2008: North Pacific Gyre Oscillation links ocean climate and ecosystem change. *Geophys. Res. Lett.*, **35**, L08607, https://doi.org/10.1029/2007GL032838.

——, K. M. Cobb, J. C. Furtado, N. Schneider, B. T. Anderson, A. Bracco, M. A. Alexander, and D. J. Vimont, 2010: Central Pacific El Niño and decadal climate change in the North Pacific Ocean. *Nat. Geosci.*, **3**, 762–765, https://doi.org/10.1038/ngeo984.

Ding, R., J. Li, Y. Tseng, and C. Ruan, 2015a: Influence of the North Pacific Victoria mode on the Pacific ITCZ summer precipitation. *J. Geophys. Res. Atmos.*, **120**, 964–979, https://doi.org/10.1002/2014JD022364.

——, ——, ——, C. Sun, and Y. Guo, 2015b: The Victoria mode in the North Pacific linking extratropical sea level pressure variations to ENSO. *J. Geophys. Res. Atmos.*, **120**, 27–45, https://doi.org/10.1002/2014JD022221.

Ding, Y., 1992: Summer monsoon rainfalls in China. *J. Meteor. Soc. Japan*, **70**, 373–396, https://doi.org/10.2151/jmsj1965.70.1B_373.

——, and J. C. L. Chan, 2005: The East Asian summer monsoon: An overview. *Meteor. Atmos. Phys.*, **89**, 117–142, https://doi.org/10.1007/s00703-005-0125-z.

——, J.-J. Liu, Y. Sun, Y.-J. Liu, J.-H. He, and Y.-F. Song, 2007: A study of the synoptic-climatology of the Meiyu system in East Asia (in Chinese). *Chin. J. Atmos. Sci.*, **31**, 1082–1101.

Dong, L., P. Guo, and F. Zhang, 2010: Relationship between variations of East Asian subtropical westerly jet from early summer to mid summer and withdrawal of Meiyu from Jianghuai region (in Chinese). *Trans. Atmos. Sci.*, **33**, 74–81.

Du, M.-X., Z.-D. Lin, and R.-Y. Lu, 2017: Combined impact of in-phase and out-of-phase variation between the northern East Asian low and western North Pacific subtropical high on East Asian summer rainfall. *Atmos. Oceanic Sci. Lett.*, **10**, 284–290, https://doi.org/10.1080/16742834.2017.1312262.

Enomoto, T., B. J. Hoskins, and Y. Matsuda, 2003: The formation mechanism of the Bonin high in August. *Quart. J. Roy. Meteor. Soc.*, **129**, 157–178, https://doi.org/10.1256/qj.01.211.

Fan, K., Z. Xu, and B. Tian, 2013: Has the intensity of the interannual variability in summer rainfall over South China remarkably increased? *Meteor. Atmos. Phys.*, **124**, 23–32, https://doi.org/10.1007/s00703-013-0301-5.

Frankignoul, C., and N. Sennechael, 2007: Observed influence of North Pacific SST anomalies on the atmospheric circulation. *J. Climate*, **20**, 592–606, https://doi.org/10.1175/JCLI4021.1.

——, ——, Y.-O. Kwon, and M. A. Alexander, 2011: Influence of the meridional shifts of the Kuroshio and the Oyashio Extensions on the atmospheric circulation. *J. Climate*, **24**, 762–777, https://doi.org/10.1175/2010JCLI3731.1.

Furtado, J. C., E. Di Lorenzo, B. T. Anderson, and N. Schneider, 2012: Linkages between the North Pacific Oscillation and central tropical Pacific SSTs at low frequencies. *Climate Dyn.*, **39**, 2833–2846, https://doi.org/10.1007/s00382-011-1245-4.

Gent, P. R., and Coauthors, 2011: The Community Climate System Model version 4. *J. Climate*, **24**, 4973–4991, https://doi.org/10.1175/2011JCLI4083.1.

Gu, W., C. Li, X. Wang, W. Zhou, and W. Li, 2009: Linkage between mei-yu precipitation and North Atlantic SST on the decadal timescale. *Adv. Atmos. Sci.*, **26**, 101–108, https://doi.org/10.1007/s00376-009-0101-5.

——, L. Wang, Z.-Z. Hu, K. Hu, and Y. Li, 2018: Interannual variations of the first rainy season precipitation over South China. *J. Climate*, **31**, 623–640, https://doi.org/10.1175/JCLI-D-17-0284.1.

Guo, Q., and J. Wang, 1981: Interannual variations of rain spell during predominant summer monsoon over China for recent thirty years (in Chinese). *Acta Geogr. Sin.*, **48**, 187–195.

He, C., and T. Zhou, 2015: Decadal change of the connection between summer western North Pacific subtropical high and tropical SST in the early 1990s. *Atmos. Sci. Lett.*, **16**, 253–259, https://doi.org/10.1002/asl2.550.

Huang, B., and Coauthors, 2017: Extended Reconstructed Sea Surface Temperature, version 5 (ERSSTv5): Upgrades, validations, and intercomparisons. *J. Climate*, **30**, 8179–8205, https://doi.org/10.1175/JCLI-D-16-0836.1.

Huang, Q., L. Wang, Y. Li, and J. He, 2012: Determination of the onset and ending of regional Meiyu over Yangtze-Huaihe River valley and its characteristics. *J. Trop. Meteor.*, **28**, 749–756.

Huang, R., 1992: The East Asia–Pacific pattern teleconnection of summer circulation and climate anomaly in East Asia. *Acta Meteor. Sin.*, **6**, 25–37.

——, R. Zhang, and B. Yan, 2001: Dynamical effect of the zonal wind anomalies over the tropical western Pacific on ENSO cycles. *Sci. China Earth Sci.*, **44**, 1089–1098, https://doi.org/10.1007/BF02906865.

Jin, F.-F., 1997: A theory of interdecadal climate variability of the North Pacific Ocean–atmosphere system. *J. Climate*, **10**, 1821–1835, https://doi.org/10.1175/1520-0442(1997)010<1821:ATOICV>2.0.CO;2.

Joh, Y., and E. Di Lorenzo, 2017: Increasing coupling between NPGO and PDO leads to prolonged marine heatwaves in the northeast Pacific. *Geophys. Res. Lett.*, **44**, 11 663–11 671, https://doi.org/10.1002/2017GL075930.

Kalnay, E., and Coauthors, 1996: The NCEP/NCAR 40-Year Reanalysis Project. *Bull. Amer. Meteor. Soc.*, **77**, 437–471, https://doi.org/10.1175/1520-0477(1996)077<0437:TNYRP>2.0.CO;2.

Kay, J. E., and Coauthors, 2014: The Community Earth System Model (CESM) large ensemble project: A community resource for studying climate change in the presence of internal climate variability. *Bull. Amer. Meteor. Soc.*, **96**, 1333–1349, https://doi.org/10.1175/BAMS-D-13-00255.1.

Kuwano-Yoshida, A., B. Taguchi, and S.-P. Xie, 2013: Baiu rainband termination in atmospheric and coupled atmosphere–ocean models. *J. Climate*, **26**, 10 111–10 124, https://doi.org/10.1175/JCLI-D-13-00231.1.

Kwon, Y.-O., and C. Deser, 2007: North Pacific decadal variability in the Community Climate System Model version 2. *J. Climate*, **20**, 2416–2433, https://doi.org/10.1175/JCLI4103.1.

Lengaigne, M., E. Guilyardi, J.-P. Boulanger, C. Menkes, P. Delecluse, P. Inness, J. Cole, and J. Slingo, 2004: Triggering of El Niño by westerly wind events in a coupled general circulation model. *Climate Dyn.*, **23**, 601–620, https://doi.org/10.1007/s00382-004-0457-2.

Li, H., S. He, K. Fan, and H. Wang, 2019: Relationship between the onset date of the Meiyu and the South Asian anticyclone in April and the related mechanisms. *Climate Dyn.*, **52**, 209–226, https://doi.org/10.1007/s00382-018-4131-5.

Li, L., and Y. Zhang, 2014: Effects of different configurations of the East Asian subtropical and polar front jets on precipitation during the mei-yu season. *J. Climate*, **27**, 6660–6672, https://doi.org/10.1175/JCLI-D-14-00021.1.

Li, X., S. Xie, S. T. Gille, and C. Yoo, 2016: Atlantic-induced pan-tropical climate change over the past three decades. *Nat. Climate Change*, **6**, 275–279, https://doi.org/10.1038/nclimate2840.

Lin, Z., and R. Lu, 2008: Abrupt northward jump of the East Asian upper-tropospheric jet stream in mid-summer. *J. Meteor. Soc. Japan*, **86**, 857–866, https://doi.org/10.2151/jmsj.86.857.

Liu, Q., N. Wen, and Z. Liu, 2006: An observational study of the impact of the North Pacific SST on the atmosphere. *Geophys. Res. Lett.*, **33**, L18611, https://doi.org/10.1029/2006GL026082.

Liu, Y., J. Hong, C. Liu, and P. Zhang, 2013: Meiyu flooding of Huaihe River valley and anomaly of seasonal variation of subtropical anticyclone over the western Pacific. *Chin. J. Atmos. Sci.*, **37**, 439–450.

Lu, R., H. Ye, and J.-G. Jhun, 2011: Weakening of interannual variability in the summer East Asian upper-tropospheric westerly jet since the mid-1990s. *Adv. Atmos. Sci.*, **28**, 1246–1258, https://doi.org/10.1007/s00376-011-0222-5.

Mantua, N. J., and S. R. Hare, 2002: The Pacific decadal oscillation. *J. Oceanogr.*, **58**, 35–44, https://doi.org/10.1023/A:1015820616384.

——, ——, Y. Zhang, J. M. Wallace, and R. C. Francis, 1997: A pacific interdecadal climate oscillation with impacts on salmon production. *Bull. Amer. Meteor. Soc.*, **78**, 1069–1080, https://doi.org/10.1175/1520-0477(1997)078<1069:APICOW>2.0.CO;2.

Matsumura, S., S. Sugimoto, and T. Sato, 2015: Recent intensification of the western Pacific subtropical high associated with the East Asian summer monsoon. *J. Climate*, **28**, 2873–2883, https://doi.org/10.1175/JCLI-D-14-00569.1.

——, T. Horinouchi, S. Sugimoto, and T. Sato, 2016: Response of the baiu rainband to northwest Pacific SST anomalies and its impact on atmospheric circulation. *J. Climate*, **29**, 3075–3093, https://doi.org/10.1175/JCLI-D-15-0691.1.

McGregor, S., A. Timmermann, M. F. Stuecker, M. H. England, M. A. Merrifield, F. Jin, and Y. Chikamoto, 2014: Recent Walker circulation strengthening and Pacific cooling amplified by Atlantic warming. *Nat. Climate Change*, **4**, 888–892, https://doi.org/10.1038/nclimate2330.

Miller, A. J., and N. Schneider, 2000: Interdecadal climate regime dynamics in the North Pacific Ocean: Theories, observations, and ecosystem impacts. *Prog. Oceanogr.*, **47**, 355–379, https://doi.org/10.1016/S0079-6611(00)00044-6.

Nakamura, T., Y. Tachibana, M. Honda, and S. Yamane, 2006: Influence of the Northern Hemisphere annular mode on ENSO by modulating westerly wind bursts. *Geophys. Res. Lett.*, **33**, L07709, https://doi.org/10.1029/2005GL025432.

North, G. R., T. Bell, R. Cahalan, and F. Moeng, 1982: Sampling errors in the estimation of empirical orthogonal functions. *Mon. Wea. Rev.*, **110**, 699–706, https://doi.org/10.1175/1520-0493(1982)110<0699:SEITEO>2.0.CO;2.

Qian, W., J. Zhu, Y. Wang, and J. Fu, 2008: Regional relationship between the Jiang-Huai Meiyu and the equatorial surface-subsurface temperature anomalies. *Chin. Sci. Bull.*, **54**, 79–84.

Rogers, J. C., 1981: The North Pacific Oscillation. *J. Climatol.*, **1**, 39–57, https://doi.org/10.1002/joc.3370010106.

Su, T., F. Xue, M. Chen, and X. Dong, 2017: A mechanism study for intraseasonal oscillation impact on the two northward jumps of the western Pacific subtropical high. *Chin. J. Atmos. Sci.*, **41**, 437–460.

Sun, B., H. Wang, B. Zhou, and H. Li, 2019: Interdecadal variation in the synoptic features of mei-yu in the Yangtze River valley region and relationship with the Pacific decadal oscillation. *J. Climate*, **32**, 6251–6270, https://doi.org/10.1175/JCLI-D-19-0017.1.

Sun, J., W. Yuan, and Y. Gao, 2008: Arabian Peninsula–North Pacific Oscillation and its association with the Asian summer monsoon. *Sci. China*, **51D**, 1001–1012, https://doi.org/10.1007/s11430-008-0058-8.

Tanaka, M., 1992: Interseasonal and interannual oscillation and the onset and retreat dates of the summer monsoon over East, Southeast Asia and the Western Pacific region using GMS high cloud amount data. *J. Meteor. Soc. Japan*, **70**, 613–629, https://doi.org/10.2151/jmsj1965.70.1B_613.

Tao, S. Y., and L. X. Chen, 1987: A review of recent research on the East Asian summer monsoon in China. *Monsoon Meteorology*, Oxford University Press, 60–92.

Trenberth, K. E., 1990: Recent observed interdecadal climate changes in the Northern Hemisphere. *Bull. Amer. Meteor. Soc.*, **71**, 988–993, https://doi.org/10.1175/1520-0477(1990)071<0988:ROICCI>2.0.CO;2.

Vimont, D. J., D. S. Battisti, and A. C. Hirst, 2003: The seasonal footprinting mechanism in the CSIRO general circulation models. *J. Climate*, **16**, 2653–2667, https://doi.org/10.1175/1520-0442(2003)016<2653:TSFMIT>2.0.CO;2.

Wang, B., and LinHo, 2002: Rainy season of the Asian–Pacific summer monsoon. *J. Climate*, **15**, 386–398, https://doi.org/10.1175/1520-0442(2002)015<0386:RSOTAP>2.0.CO;2.

Wang, C., and L. Wang, 2018: Combined effects of synoptic-scale teleconnection patterns on summer precipitation in southern China. *Atmosphere*, **9**, 154, https://doi.org/10.3390/atmos9040154.

Wang, L., Z. Guan, and J. He, 2006: The position variation of the western Pacific subtropical high and its possible mechanism. *J. Trop. Meteor.*, **12**, 113–120.

——, H. Gao, Z. Guan, and J. He, 2011: Relationship between the western Pacific subtropical high and the subtropical East Asian diabatic heating during south China heavy rains in June 2005. *Acta Meteor. Sin.*, **25**, 203–210, https://doi.org/10.1007/s13351-011-0027-6.

Wang, S., Z. Zhao, D. Gong, and T. Zhou, 2005: *Introduction of Climatology*. China Meteorological Press, 43 pp.

Wu, J., and X. Gao, 2013: A gridded daily observation dataset over China region and comparison with the other datasets. *Chin. J. Geophys.*, **56**, 1102–1111.

Wu, L., Z. Liu, C. Li, and Y. Sun, 2006: Extratropical control of recent tropical Pacific decadal climate variability: A relay teleconnection. *Climate Dyn.*, **28**, 99–112, https://doi.org/10.1007/s00382-006-0198-5.

Wu, M., and L. Wang, 2019: Enhanced correlation between ENSO and western North Pacific monsoon during boreal summer around the 1990s. *Atmos. Oceanic Sci. Lett.*, **12**, 376–384, https://doi.org/10.1080/16742834.2019.1641397.

Xiao, D., and J. Li, 2007: Spatial and temporal characteristics of the decadal abrupt changes of global atmosphere–ocean system in the 1970s. *J. Geophys. Res.*, **112**, D24S22, https://doi.org/10.1029/2007JD008956.

Xie, S.-P., K. Hu, J. Hafner, H. Tokinaga, Y. Du, G. Huang, and T. Sampe, 2009: Indian Ocean capacitor effect on Indo–western Pacific climate during the summer following El Niño. *J. Climate*, **22**, 730–747, https://doi.org/10.1175/2008JCLI2544.1.

Xie, W., G. Fan, R. Ding, J. Li, B. Li, J. Qin, and X. Zhou, 2019: Interdecadal change in the lagged relationship between the Victoria mode and ENSO. *Atmos. Oceanic Sci. Lett.*, **12**, 294–301, https://doi.org/10.1080/16742834.2019.1620081.

Xu, K., and R. Lu, 2018: Decadal change of the western North Pacific summer monsoon break around 2002/03. *J. Climate*, **31**, 177–193, https://doi.org/10.1175/JCLI-D-16-0739.1.

Yanai, M., S. Esbensen, and J.-H. Chu, 1973: Determination of bulk properties of tropical cloud clusters from large-scale heat and moisture budgets. *J. Atmos. Sci.*, **30**, 611–627, https://doi.org/10.1175/1520-0469(1973)030<0611:DOBPOT>2.0.CO;2.

Yao, Y., H. Lin, and Q. Wu, 2019: Linkage between interannual variation of the East Asian intraseasonal oscillation and meiyu onset. *J. Climate*, **32**, 145–160, https://doi.org/10.1175/JCLI-D-17-0873.1.

Ye, M., and H. Chen, 2019: Recognition of two dominant modes of EASM and its thermal driving factors based on 25 monsoon indexes. *Atmos. Oceanic Sci. Lett.*, **12**, 278–285, https://doi.org/10.1080/16742834.2019.1614424.

Yeh, S.-W., Y.-J. Kang, Y. Noh, and A. J. Miller, 2011: The North Pacific climate transitions of the winters of 1976/77 and 1988/89. *J. Climate*, **24**, 1170–1183, https://doi.org/10.1175/2010JCLI3325.1.

Yu, P., L. Zhang, and Q. Zhong, 2016: An interdecadal change in the relationship between the western North Pacific Ocean and the East Asian summer monsoon. *Climate Dyn.*, **49**, 1139–1156, https://doi.org/10.1007/s00382-016-3370-6.

——, ——, and ——, 2018: Contrasting relationship between the Kuroshio Extension and the East Asian summer monsoon before and after the late 1980s. *Climate Dyn.*, **52**, 929–950, https://doi.org/10.1007/s00382-018-4173-8.

Yun, K.-S., K.-H. Seo, and K.-J. Ha, 2010: Interdecadal change in the relationship between ENSO and the intraseasonal oscillation in East Asia. *J. Climate*, **23**, 3599–3612, https://doi.org/10.1175/2010JCLI3431.1.

Zhang, J., and Coauthors, 2018: Stratospheric ozone loss over the Eurasian continent induced by the polar vortex shift. *Nat. Commun.*, **9**, 206, https://doi.org/10.1038/s41467-017-02565-2.

Zhang, L., P. Chang, and L. Ji, 2009a: Linking the Pacific meridional mode to ENSO: Coupled model analysis. *J. Climate*, **22**, 3488–3505, https://doi.org/10.1175/2008JCLI2473.1.

——, ——, and M. K. Tippett, 2009b: Linking the Pacific meridional mode to ENSO: Utilization of a noise filter. *J. Climate*, **22**, 905–922, https://doi.org/10.1175/2008JCLI2474.1.

Zhao, J., L. Chen, and D. Wang, 2018: Characteristics and causes analysis of abnormal Meiyu in China in 2016. *Chin. J. Atmos. Sci.*, **42**, 1055–1066.

Zhao, W., S. Chen, W. Chen, S. Yao, D. Nath, and B. Yu, 2019: Interannual variations of the rainy season withdrawal of the monsoon transitional zone in China. *Climate Dyn.*, **53**, 2031–2046, https://doi.org/10.1007/s00382-019-04762-9.

Zheng, J., J. Li, and J. Feng, 2014: A dipole pattern in the Indian and Pacific Oceans and its relationship with the East Asian summer monsoon. *Environ. Res. Lett.*, **9**, 074006, https://doi.org/10.1088/1748-9326/9/7/074006.

——, D. Sun, K. Liu, Z. Hao, X. Zhang, and Q. Ge, 2016: Variations of extreme Meiyu events and flood disasters over the mid-lower reaches of the Yangtze River for the past 300 years. *J. Nat. Resour.*, **31**, 1971–1983.

Zhu, Y., H. Wang, W. Zhou, and J. Ma, 2011: Recent changes in the summer precipitation pattern in East China and the background circulation. *Climate Dyn.*, **36**, 1463–1473, https://doi.org/10.1007/s00382-010-0852-9.

——, ——, J. Ma, T. Wang, and J. Sun, 2015: Contribution of the phase transition of Pacific decadal oscillation to the late 1990s' shift in East China summer rainfall. *J. Geophys. Res. Atmos.*, **120**, 8817–8827, https://doi.org/10.1002/2015JD023545.

Zuo, J., W. Li, C. Sun, and H. Ren, 2019: Remote forcing of the northern tropical Atlantic SST anomalies on the western North Pacific anomalous anticyclone. *Climate Dyn.*, **52**, 2837–2853, https://doi.org/10.1007/s00382-018-4298-9.